Biomechanics and Modeling in Mechanobiology (2020) 19:2127–2147
https://doi.org/10.1007/s10237-020-01328-1

ORIGINAL PAPER

An efficient two-scale 3D FE model of the bone fibril array: comparison of anisotropic elastic properties with analytical methods and micro-sample testing

Elham Alizadeh[1] · **Mehdi Dehestani**[1] · **Philippe Zysset**[2]

Received: 28 December 2019 / Accepted: 11 April 2020 / Published online: 24 April 2020

Abstract
In this study, 3D finite element analyses (FEA) are conducted to quantify the orthotropic elastic properties and investigate the load transfer mechanism of bone at the sub-lamellar level. Three finite element (FE) unit cells with periodic boundary conditions are presented to model a two-scale microstructure of bone including a mineralized collagen fibril (MCF), the extrafibrillar matrix (EFM) and the resulting fibril array (FAY) under arbitrary loading. The axial and transverse elastic properties of the FAY computed by FEA are calibrated with unique experimental results on ovine micro-samples showing a coherent fibril orientation. They are then systematically compared with those calculated using analytical methods including the basic Voigt, Reuss and shear-lag models, the Mori–Tanaka scheme and the upper and lower bounds by Hashin and Shtrikman. The predicted axial strain ratios between the two-scales are discussed with respect to a recent small-angle X-ray scattering and wide-angle X-ray diffraction study. Beyond apparent elastic properties, the FE models provide stress distributions at both hierarchical levels, confirm the shear lag mechanisms within the MCF and between MCF and EFM and identify potential damage sites under arbitrary loading conditions. A comprehensive sensitivity analysis shows that mineral volume fraction in the fibril array is the dominant parameter on the axial and transverse elastic moduli, while the MCF volume fraction in FAY is the most sensitive variable for the ratio of axial versus transverse elastic modulus followed by the elastic moduli of hydroxyapatite and collagen. The FE model of the FAY developed and calibrated in the current study represents an anatomically realistic, experimentally validated and computationally efficient basis for investigating the apparent yield, post-yield and failure behaviors of lamellar bone in future research.

Keywords Anisotropic elasticity · Extracellular matrix · Finite element model · Mineralized collagen fibril · Extrafibrillar matrix · Sensitivity analysis

1 Introduction

Bone is a mineralized biological tissue that provides structural support and stability, stores minerals, produces blood cells and protects vital internal organs (Weiner et al. 1999; Fratzl and Weinkamer 2007). The hierarchical structure of bone is subdivided into several scales from nano to macro (Fig. 1) (Rho et al. 1998; Reznikov et al. 2014), and the optimized arrangement of its constituents forms a lightweight composite material with high stiffness, strength and fracture toughness (Weiner et al.1999). At the nanoscale, the mineralized collagen fibril (MCF) is made of collagen, hydroxyapatite (HA) crystals and water and is regarded as the primary building block of bone extracellular matrix (ECM) (Olszta et al. 2007; Minary-Jolandan and Yu 2009a; Hang and Barber 2010). Mineralized collagen fibrils embedded in extrafibrillar matrix (EFM) combine into fibril arrays at the microscale (Currey 2013). At the next scale of a few to hundreds of microns, random arrangements of these arrays form woven bone, while orthogonal, twisted and other arrangements of fibril arrays (FAY) form lamellae constituting the lamellar bone found in bone structural units (BSU) such as osteons or trabecular packets and in circumferential lamellae at the periosteal/endosteal surfaces

✉ Mehdi Dehestani
dehestani@gmail.com

[1] Department of Civil Engineering (Structural Engineering), Babol Noshirvani University of Technology, Babol, Iran

[2] ARTORG Centre for Biomedical Engineering Research, University of Bern, Bern, Switzerland

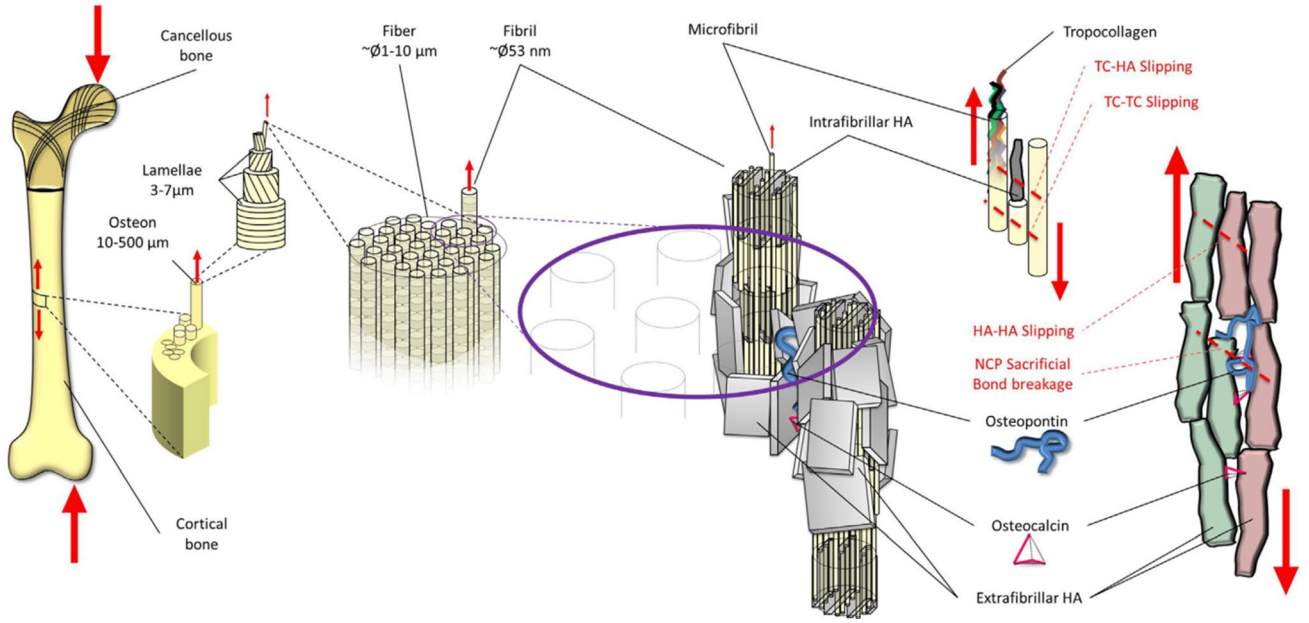

Fig.1 Hierarchical structure of cortical bone (Nikel et al. 2018)

of compact bone (Giraud-Guille 1988; Akiva et al. 1998). At the mesoscale between several hundred microns and millimeters, the osteons form cylindrical lamellar systems around a Haversian channel, while trabecular packets build a 3D microstructure of beams and plates surrounded by marrow. In the course of the bone remodeling process, the osteons and trabecular packets overlap interstitial lamellae from former bone structural units (Aoubiza et al. 1996; Dong and Guo 2006; Parnell and Grimal 2008). Correspondingly, the macroscale ranges from millimeters to centimeters, denoting the whole bone level (Currey 2013).

In general, investigation of bone mechanical properties aims to a better understanding of fragility and failure of the bone-implant interface. Besides, the acquired knowledge may be utilized to design and develop novel composite materials to be used in biomedical engineering applications (Cassella et al. 1996; Fratzl-Zelman et al. 2014; Bishop 2016; Paschalis et al. 2016). Numerous methods are used to model the multi-scale mechanical properties of bone such as structural and continuum mechanics, micromechanics, finite element analysis (FEA) and molecular dynamics (MD). However, only few experimental methods are available to measure model parameters at the lower scales. Accordingly, the MCF/EFM and FAY levels are considered in this study and several modeling strategies and experiments on these two-scales are briefly reviewed in the following section.

Basic models including Voigt (1889) and Reuss (1929) consider the bone composite as a material consisting of matrix and fiber phases and estimate the apparent axial or transverse elastic properties with regard to volume fraction and elastic modulus of the constituents under uniform strain and stress, respectively (Cox 1952; Hirsch 1962; Hashin and Shtrikman 1963; Currey 1969; Padawer and Beecher 1970; Katz 1971; Lusis et al. 1973; Piekarski 1973; Halpin and Kardos 1976; Wagner and Weiner 1992; Wall 1997). Jäger and Fratzl (2000) proposed a model of MCF with a staggered arrangement of HA platelets in collagen fibrils, known as the shear-lag model which was then exploited by Gao et al. (2003) to calculate the longitudinal elastic modulus of bone.

Based on continuum micromechanics theory, Mori and Tanaka (MT) (Mori and Tanaka 1973; Benveniste 1987) derived equations to compute the effective elastic modulus of matrix-inclusion composite materials. The self-consistent (SC) method is another micromechanical approach proposed by Hershey (1954) and Kröner (1958) for polycrystalline aggregates which was further developed by Hill (1963) and Budiansky (1965) for composite materials. Both MT and SC methods were employed to estimate the elastic properties of bone at MCF, EFM and FAY levels (Hellmich et al. 2004; Fritsch and Hellmich 2007; Nikolov and Raabe 2008; Hamed et al. 2010; Reisinger et al. 2010).

Ji and Gao (2004) computed the elastic properties of MCF by FEA based on a shear-lag geometry, while Yuan et al. (2011) developed 2D and 3D FE models to determine the effect of collagen and HA modulus, mineral volume fraction, and thickness of mineral platelets on the MCF longitudinal modulus. Barkaoui and Hambli (2011, 2014) assessed the elastic modulus of a 3D FE model of the mineralized collagen microfibril containing five tropocollagen molecules linked together with springs, while the entire structure was embedded in a mineral matrix. They also calculated the

multi-scale elastic properties of bone ECM using neural networks trained with FEM at the nanoscale and homogenization theory at higher scales (Barkaoui et al. 2014, 2016). As suggested by Vercher-Martínez et al. (2015), the effect of mineral staggering on the elastic modulus of MCF can be determined by changing the longitudinal and transverse distance of minerals as well as rotating the mineral platelets in the FE model. Schwarcz et al. (2017) and Abueidda et al. (2017) modeled the nanostructure of bone with a new collagen-mineral arrangement (McNally et al. 2012, 2013; Schwarcz et al. 2014) where mineral platelets coat the outer surfaces of collagen fibrils and compared the resulting elastic properties with those models in which mineral platelets are distributed within collagen fibrils (Jäger and Fratzl 2000). Maghsoudi-Ganjeh et al. (2019) proposed a 2D cohesive FE model of the FAY that reveals damage initiation mechanisms under compression and tension. Wang and Ural (2018) used a 3D statistical model of the FAY to investigate the influence of size and orientation of MCFs on the mechanical response under transverse and longitudinal loading. Many of these FE models involve a large number of unverifiable assumptions, require large computational resources, lack comparison with previous analytical models, and miss experimental validation at the proper hierarchical levels.

At the molecular level, MD methods are used to explore the mechanical properties of collagen fibrils in the absence or presence of mineral platelets, but do not include the EFM yet (Lorenzo and Caffarena 2005; Buehler 2006, 2007, 2008; Bhowmik et al. 2007; Dubey and Tomar 2008; Stevens 2008; Tang et al. 2009; Gautieri et al. 2011; Nair et al. 2013).

Quantifying the mechanical properties of bone at nano- and microscale has been the object of only few experimental methods. Asgari et al. (2019) utilized indentation by atomic force microscopy (AFM) (Wallace 2012) to measure the longitudinal and transverse elastic moduli of bone at the nanoscale. Nanoindentation was applied extensively along various anatomical orientations to quantify the anisotropic elasticity of human lamellar bone and FAYs from mineralized turkey leg tendon (Franzoso and Zysset 2009; Reisinger et al. 2011a; Spiesz and Zysset 2015). In addition to nano-indentation, Schwiedrzik et al. (2014) used micropillar compression tests in a scanning electron microscope (SEM), to measure the mechanical behavior of ovine FAYs under monotonic and cyclic loads. Tertuliano and Greer (2016) performed uniaxial compression experiments on micro- and nano-pillars to determine their mechanical properties. More recently, Casari et al. (2019a) presented a technological breakthrough to test micron-sized specimens under uniaxial tensile loading. The sample geometry was optimized by FEA and the developed micro-tensile setup self-aligned with the specimen's axis to prevent stress concentrations. This methodology was then used to quantify the tensile mechanical properties of ovine bone at the FAY level in axial and transverse directions. The obtained results were then compared to those of micropillar compression of the same tissue (Casari et al. 2019b) and revealed for the first time the strength tension–compression asymmetry of bone at the FAY level.

In the above context, the current study aims at developing simple, cost-efficient, 3D homogenized unit-cell FE models that reproduce the key stress transfer mechanism between MCF and EFM and delivers the recent experimental elastic properties of the FAY in axial and transverse directions (Casari et al. 2019b) with the best current knowledge of the compositional and dimensional properties of the bone ECM. The predictions of the FE model for axial and transverse elastic moduli are systematically compared to the ones of published analytical models for the same FAY organization. A comprehensive sensitivity analysis is then carried out in order to determine the most influential parameters on the anisotropic elastic moduli of the FAY. Following this broad validation study, the FE model will be devoted to the exploration of the basic mechanisms of damage accumulation and to the estimation of apparent post-yield properties of the bone ECM in 3D.

2 Materials and methods

In this section, the constituents and morphology of bone MCF, EFM and FAY are presented and the details of the FE models, their experimental calibration, their sensitivity analysis and the analytical models utilized for comparison are described.

2.1 Constituents

Bone is a natural composite comprising an inorganic phase, an organic phase and water. The inorganic phase of bone mainly consists of mineral platelets with a chemical composition based on hydroxyapatite (HA),$Ca_5(PO_4)_3OH$, subjected to multiple ion substitutions (Cowin 2001; Dubey and Tomar 2008). Small-angle X-ray scattering (SAXS) (Fratzl et al. 1992; Paris et al. 2000; Fratzl 2003), transmission electron microscopy (TEM) (Weiner and Traub 1992; Landis 1996; Landis et al. 1996) and scanning TEM (STEM) tomography (Reznikov et al. 2018) have typically been used to determine the shape and size of mineral crystals. The results suggested an approximately plate-like shape in mineralized turkey leg tendons (MTLT) and human bone (Robinson 1952; Jackson et al. 1978; landis and Price 1986; Traub et al. 1989; MJ and BF 1993; Lees et al. 1994; Prostak and Lees 1996; Rubin et al. 2003), and a needle-like geometry in mouse, rat, dog and horse bone (Fratzl et al. 1992, 1996). In this regard, an AFM study confirmed that HA crystals in bovine bone have a plate-like shape (Eppell

et al. 2001) and researchers reported a range of HA thickness from 2 to 7 nm, a length from 15 to 200 nm and a width from 10 to 80 nm (Landis and Silver 2002; Rubin et al. 2003; Vercher-Martínez et al. 2015). The elastic modulus of HA platelets is reported in the range of 80–120 GPa (Ravaglioli and Krajewski 1991; Amaral et al. 2002), and wet mineral density is approximately 3.1 g/cm^3 (Lees 1987; Hellmich et al. 2004).

Collagen type I represents 90% of the organic phase in bone, comprises chains with repetitive amino acid sequences and assembles into a triple helical structure called tropocollagen. The formation of covalent cross-links between collagen molecules contributes to a self-organization into collagen fibrils (Rice et al. 1964; Miller 1984; Parry 1988; Kadler et al. 1996; Fratzl et al. 2004; Buehler 2008). The collagen fibril follows a staggered arrangement with a 67 nm periodicity composed of a 40 nm gap zone and a 27 nm overlap zone (Katz and Li 1973a, b; Weiner and Traub 1986; Landis et al. 1993; Rho et al. 1998; Orgel et al. 2001). It is noteworthy that the density of wet collagen is approximately 1.18 g/cm^3 (Piekarski 1973; Cusack and Miller 1979; Deuerling et al. 2009; Gautieri et al. 2011). The mechanical properties of collagen fibrils can be measured experimentally or calculated bottom up by MD (Eppell et al. 2005; Heim et al. 2006; Van Der Rijt et al. 2006; Wenger et al. 2007; Yang et al. 2007). A wide range of elastic moduli of collagen from 0.2 up to 21 GPa are reported in the literature (Harley et al. 1977; Cusack and Miller 1979; Hofmann et al. 1984; Sasaki and Odajima 1996; Eppell et al. 2005; Lorenzo and Caffarena 2005; Vesentini et al.2005; Buehler 2006; Heim et al. 2006; Van Der Rijt et al. 2006; Yang et al. 2007, 2008; Wenger et al. 2007; Grant et al. 2008; Minary-Jolandan and Yu 2009b; Shen et al. 2010). The elastic modulus of collagen fibrils depends on the experimental technique, collagen orientation and hydration state, but a value between 5 and 7 GPa seems realistic in continuum models (Reisinger et al. 2010).

The non-collagenous protein (NCP) constitutes the remaining 10% of the organic phase which consists of osteopontin, osteocalcin, osteonectin, phosphoproteins, bone sialoproteins and proteoglycans (Mbuyi-Muamba et al. 1989; Kasugai et al. 1991; Ingram et al. 1993; Roach 1994; Cribb and Scott 1995; Nanci 1999; Raspanti et al. 2002; Hansma et al. 2005; Fantner et al. 2007; Wise et al. 2007; Thurner 2009; Urist and Strates 2009; Sroga and Vashishth 2012; Al-Qtaitat and Aldalaen 2014). The NCPs control mineral crystal nucleation and also regulate its growth, size, orientation and morphology. In addition, NCPs may allow the relative sliding of mineral crystals and play an important role in plasticity, toughening and energy dissipation of bone (Mann et al. 1989; Boskey 1992; Qiu et al. 2004; Fantner et al. 2005; Adams et al. 2008; Buehler et al. 2008; Zappone et al. 2008; Huang et al. 2009; Poundarik et al. 2009,2012; Ritchie et al. 2009; Thurner et al. 2010; Nikel et al. 2013; Hang et al. 2014; Morgan et al. 2015). For simplicity, the density of wet NCPs is considered similar to that of the collagen phase in this study, i.e., 1.18 g/cm^3. Unfortunately, the mechanical properties of NCPs are widely unknown. Due to their flexible coiling configuration, the elastic modulus of NPCs must be lower than the one of collagen and was assumed to be equal/lower than 1 GPa in previous research (Nikolov and Raabe 2008; Hamed et al. 2012). The mineral platelet and collagen type I are the main constituents of the mineralized collagen fibril (MCF), while HA crystals and NCPs are the building blocks of the extrafibrillar matrix (EFM). The aspect ratio of mineral crystals is reported to range from 30 to 40 in bone (Gao et al. 2003). However, some studies considered a mineral aspect ratio of 14, respecting the 40 nm length of HA crystals deposited in the gap zone between collagen fibrils divided by the 3 nm thickness of platelets (Akkus 2005; Reisinger et al. 2010; Maghsoudi-Ganjeh et al. 2019). Therefore, the mineral platelet aspect ratio has been cited from 14 up to 45 in different studies (Siegmund et al. 2008; Vercher-Martínez et al. 2015). The reported mineral content in the interfibrillar and extrafibrillar spaces diverges among researchers; however, most publications indicate that the amount of mineral in the MCF reaches 70% (Katz and Li 1973b; Sasaki and Sudoh 1997; Jäger and Fratzl 2000; Nikolov and Raabe 2008). Alexander et al. (2012) determined the amount of mineral in the gap zones of collagen fibrils by steric models and STEM. Their results suggested that HA minerals, distributed in the gap zone and intermolecular overlap region of interafibrillar matrix, are, respectively, 42 and 28% of the total HA minerals. Hence, their models claimed that 30% of the bone mineral is located in the EFM. In contrast, some other AFM and SAXS studies on turkey leg tendon and horse bone suggested the presence of approximately 70% of total HA crystals in the EFM (Lees et al. 1994; Fratzl et al. 1996).

The MCF and EFM assemble to form FAYs (Weiner and Traub 1992; Rho et al. 1998; Fratzl and Weinkamer 2007) with a high aspect ratio (Birk et al. 1997; Silver et al. 2003; Hassenkam et al. 2004; Wallace 2012). The volume fraction of MCF in the fibril array varies between 0.2 and 0.9 (Jasiuk and Ostoja-Starzewski 2004; Nikolov and Raabe 2008; Reisinger et al. 2010), while the total mineral volume fraction in the fibril array ranges from 0.15 to 0.52 (Gupta et al 2006; Nikolov and Raabe 2008; Reisinger et al. 2010; Barkaoui et al. 2014, 2015; Maghsoudi-Ganjeh et al. 2019).

The elastic modulus of plate-like mineral crystals is considered to be 110 GPa, and Young's modulus of collagen and NCP is assumed to be 6 GPa and 0.6 GPa, respectively. The mineral volume fraction in MCF and the total mineral volume fraction in the fibril array is assigned in this work to be 0.296 and 0.423, respectively. Besides, the NCP volume fraction in EFM is 0.069. The volume fraction of the MCF in the FAY

is assumed to be 0.8. Moreover, aspect ratios of 30 and 100 are specified for the mineral platelets in the MCF and for the MCF inclusions in the FAY, respectively. It is important to mention that free water is not modeled as a separate phase in this study, assuming that all water is integrated in the organic phases. The values of the input parameters of the FE models are summarized in Table 1.

2.2 Finite element analysis

In this section, a two-scale model of bone ECM including mineralized collagen fibril (MCF), extrafibrillar matrix (EFM) and fibril array (FAY) is presented to evaluate the apparent elastic properties of bone at these two-scales. The results of MCF and EFM models are used as inputs for the FAY. In order to reduce the numerical simulation costs, representative volume elements (RVE) in the form of unit cells and periodic boundary conditions (PBC) are employed (Wu et al. 2014). The unit cells were designed with the above dimensions along the existing planes of symmetry, meshed with hexahedral elements and the nodal sets of their boundary surfaces identified to apply the desired periodic boundary conditions. In order to compute the apparent elasticity tensors of MCF, EFM and FAY, the models are analyzed in three normal and three shear loading cases (Reisinger et al. 2011b). The numerical analyses are performed with the FE software ABAQUS (Hibbitt 2013), and the morphological and mechanical properties of the constituents are based on Sect. 2.1. The details of the unit cells and their analyses are now described in the following sections.

2.2.1 Mineralized collagen fibril

The unit cell model of the MCF containing hydroxyapatite platelets and collagen is shown in Fig. 2. The HA platelet is supposed to have a length of l, a width of w and a thickness of d. In addition, the distances between the mineral crystals in X, Y and Z directions are denoted by b, r, and a, respectively. In the proposed model, the mineral crystals are situated in a staggered array with a periodicity of 67 nm. The length of HA crystals (l) is taken to be 110 nm, and the lateral distance in Z direction (a) is calculated based on Eq. (1).

$$\frac{l+a}{2} = 67 \text{ nm} \tag{1}$$

As shown in Eq. (2), the aspect ratio of HA crystals (ρ) is considered 30 in this study and the thickness of minerals (d) is obtained, consequently.

$$\rho = \frac{l}{d} \tag{2}$$

A volume fraction of 0.4 is adopted for the overlap region $\left(\varphi_{\text{Overlap}-xz}\right)$ and the lateral distance in X direction (b) is calculated according to Eq. (3). Besides, the width of HA platelets (w) is computed by Eq. (4).

$$\varphi_{\text{Overlap}-xz} = \frac{(l-a)d}{(l+a)(b+d)} \rightarrow b = \left(\frac{(l-a)}{(l+a)\varphi_{\text{Overlap}-xz}} - 1\right)d \tag{3}$$

$$w = \frac{l}{2} \tag{4}$$

The volume fraction of mineral crystals in MCF $\left(\varphi_{\text{HA (MCF)}}\right)$ is 0.296, and the lateral distance between minerals in Y direction (r) is provided by Eq. (5).

$$\varphi_{\text{HA (MCF)}} = \frac{1}{\left(1+\frac{a}{l}\right)\left(1+\frac{b}{d}\right)\left(1+\frac{r}{w}\right)} \tag{5}$$

The geometrical parameters of the model, selected based on the above constraints are given in Table 2. The assumptions and the geometrical parameters are in the range of values reported in Sect. 2.1.

The mineralized collagen fibril is modeled with 8-node linear brick elements (C3D8) including eight nodes with three translational degrees of freedom at each node. Based on a mesh convergence study, the adopted mesh size has a maximum element size of 2 nm and is shown in Fig. 2.

2.2.2 Extrafibrillar matrix

For simplicity, a cubic model is assumed for the extrafibrillar matrix with a cubic HA crystal in a cubic unit cell as illustrated in Fig. 3. The volume fraction of mineral crystals in EFM is assumed to be 0.93, and the aspect ratio of HA platelet is 1. The cubic mineral inclusion is embedded in an NCP phase, filling the space between the two cubes. The mesh is based on a 0.3 nm element size and the same C3D8 element type.

2.2.3 Fibril array

A hexagonal array is selected for modeling the FAY and the rectangular unit cell with circular MCFs surrounded by EFM is shown in Fig. 4. The MCF region in the FAY model includes a central circle and four quarters of circles in the corners. An aspect ratio of 100 is assumed for MCF, and its length is calculated accordingly. It is assumed that there are gap zones in the middle part and at the end of the MCF that are filled with EFM (Fig. 5). Likewise, a volume fraction of 0.8 is assumed for the MCF in the FAY. In order to achieve a hexagonal pattern in the fibril array, the height of rectangular unit cell is considered $\sqrt{3}$ times its width and the cross-sectional dimension of the fibril

Table 1 Input parameters

Variable with physical unit ()	Symbol	Value of parameters in this study	Range of parameters in the literature	References
Elastic modulus of HA (GPa)	E_{HA}	110	80–120	Ravaglioli and Krajewski (1991) and Amaral et al. (2002)
Poisson's ratio of HA (–)	ν_{HA}	0.28	–	Katz and Ukraincik (1971), Yao et al. (2007), Siegmund et al. (2008) and Maghsoudi-Ganjeh et al. (2019)
Elastic modulus of collagen (GPa)	$E_{Collagen}$	6	0.2–21	Lorenzo and Caffarena (2005), Vesentini et al. (2005) and Buehler (2006)
Poisson's ratio of collagen (–)	$\nu_{Collagen}$	0.3	–	Reisinger et al. (2010), Vercher et al. (2014) and Vercher-Martínez et al. (2015)
Elastic modulus of NCP (GPa)	E_{NCP}	0.6	≤ 1	Nikolov and Raabe (2008) and Hamed et al. (2012)
Poisson's ratio of NCP (–)	ν_{NCP}	0.3	–	–
Volume fraction of MCF in fibril array (–)	φ_{MCF}	0.8	0.2–0.9	Jasiuk and Ostoja-Starzewski (2004) and Nikolov and Raabe (2008)
Volume fraction of HA in fibril array (–)	φ_{HA}	0.423	0.15–0.52	Barkaoui et al. (2014, 2015) and Maghsoudi-Ganjeh et al. (2019)
Volume fraction of NCP in EFM (–)	$\varphi_{NCP/EFM}$	0.069	–	–
Aspect ratio of HA (–)	a_{HA}	30	14–45	Gao et al. (2003), Siegmund et al. (2008) and Vercher-Martínez et al. (2015)
Aspect ratio of MCF in fibril array (–)	a_{MCF}	100	High value	Silver et al. (2003), Hassenkam et al. (2004) and Wallace (2012)

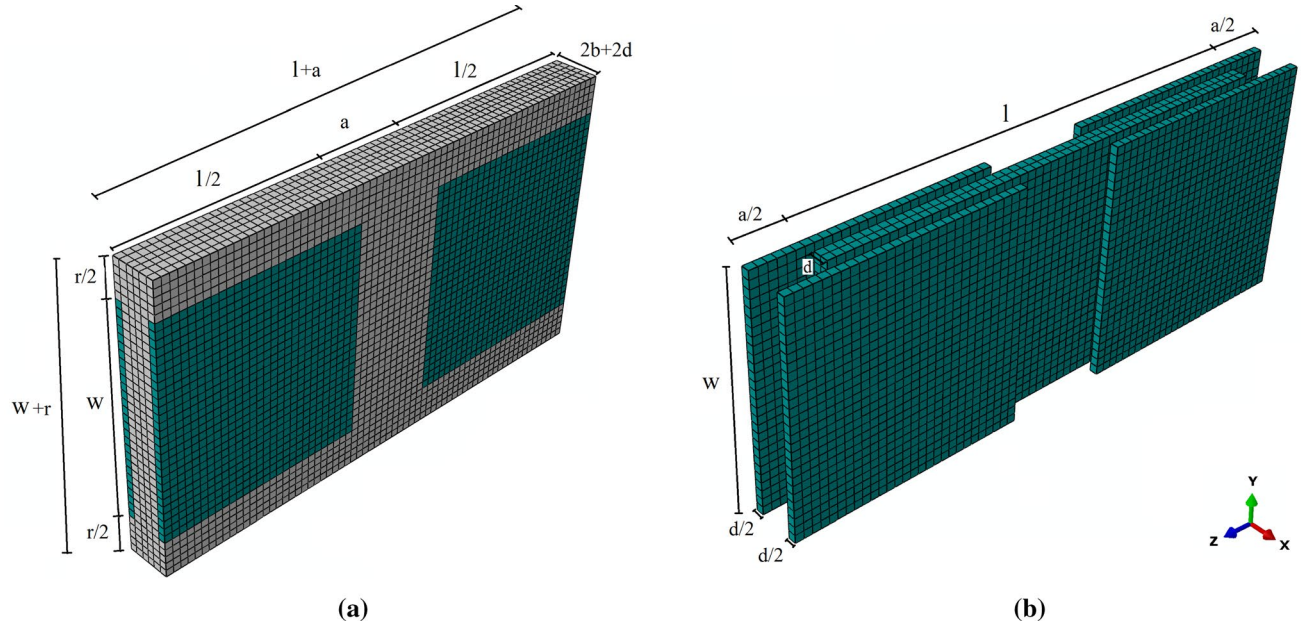

Fig. 2 Configuration of **a** MCF model, **b** mineral platelet in the MCF model

Table 2 The geometrical parameters used in modeling the MCF

Parameter	Variable	Value (nm)
Length of HA platelet	*l*	110
width of HA platelet	*w*	55
Thickness of HA platelet	*d*	3.67
Lateral distance between neighboring HA platelets in *X* direction	*b*	2.22
Lateral distance between neighboring HA platelets in *Y* direction	*r*	40.03
Longitudinal distance between neighboring HA platelets in *Z* direction	*a*	24

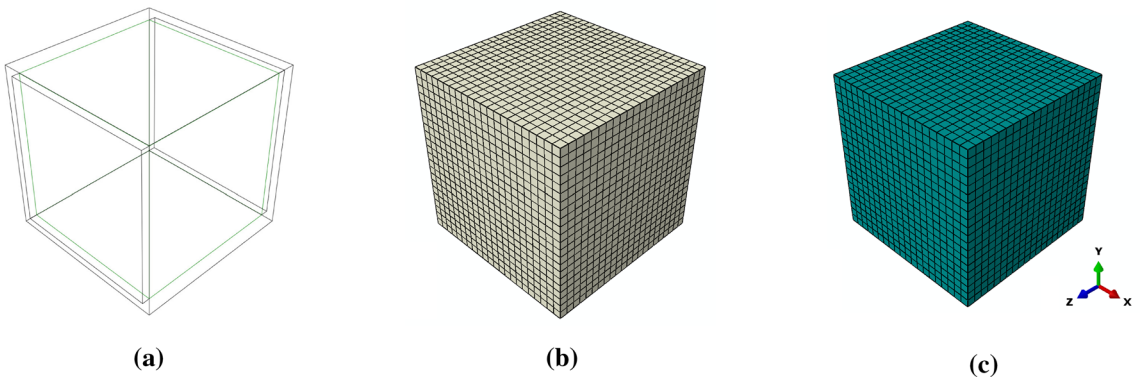

Fig. 3 **a** Two embedded cubes for EFM, **b** external part of EFM (NCP phase), **c** internal part of EFM (HA crystal)

array is calculated accordingly. The input parameters for modeling the FAY are listed in Table 3. A C3D8 element with a maximum element size of 10 nm is used in the FAY model.

The strain ratios of HA platelets in MCF, and of MCF in FAY are obtained by calculating the average axial strain of the HA elements versus the MCF elements and the MCF elements versus the average axial strain in the FAY model.

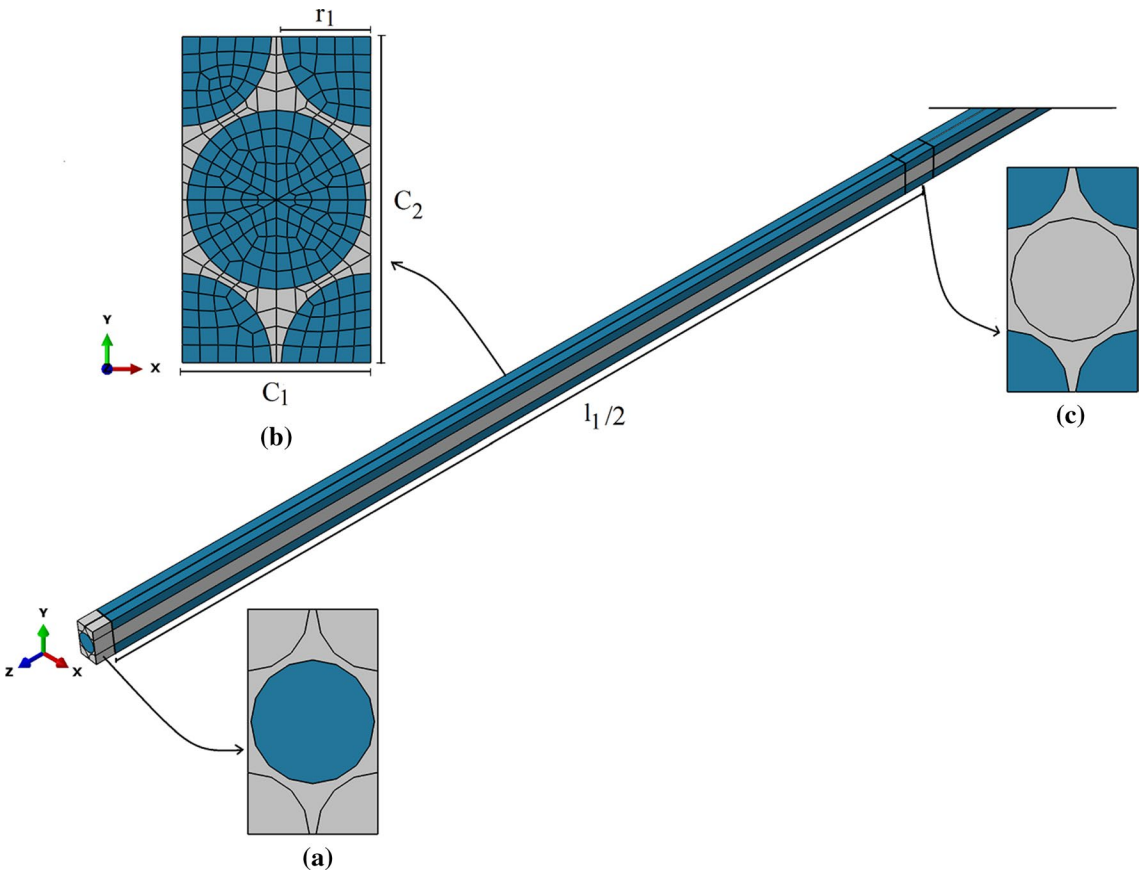

Fig. 4 Cross sections of fibril array in **a** the gap zone at the end part of FAY, **b** the length of model **c** the gap zone in the middle part of FAY (half-length of the fibril array is shown due to symmetry)

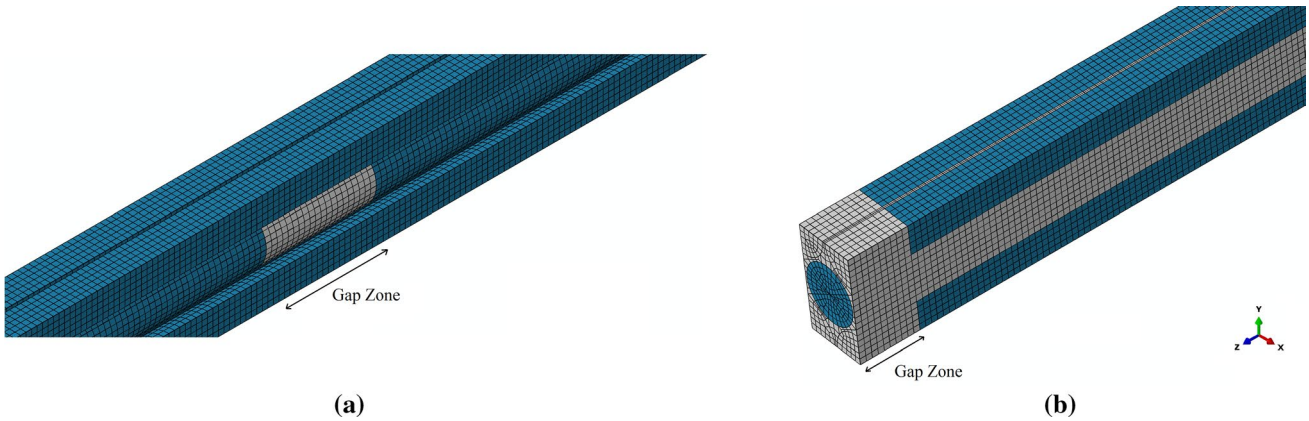

Fig. 5 **a** Gap zone in the middle part of central MCF, **b** gap zone at the end part of corner MCFs in fibril array

2.3 Calibration with experimental results

The FE analysis of the FAY model proposed in this research is calibrated with the recent experimental results obtained by Casari et al. (2019b), in which the elastic and post-yield properties of ovine bone extracellular matrix are evaluated in the axial and transverse directions. Calibration is achieved by adjusting two of the most sensitive parameters identified by Reisinger et al. 2010, namely the mineral volume fraction and the relative distribution of the mineral in MCF and EFM to minimize the difference with

Table 3 The geometrical parameters used in modeling the fibril array

Variable	Symbol	Value (nm)
Radius of MCF	r_1	50.0
Length of MCF	l_1	100×10^2
Gap region in the middle part of central MCF	l_2	200.0
Width of fibril array cross section	C_1	105.4
Height of fibril array cross section	C_2	182.0

the experimental axial and transverse moduli measured by Casari et al. (2019b) on dry ovine bone.

2.4 Parameter sensitivity analysis

The sensitivity analysis is conducted on the calibrated FAY model for the following parameters: elastic modulus of HA (E_{HA}), elastic modulus of collagen (E_{Collagen}), elastic modulus of NCP (E_{NCP}), volume fraction of MCF in FAY (φ_{MCF}), volume fraction of HA in FAY (φ_{HA}), the volume fraction of NCP in EFM (φ_{NCP} /EFM) and the aspect ratio of HA (a_{HA}). Since Poisson ratios are known to have a limited effect on composite elasticity and the aspect ratio of the MCF is already very large, these parameters were excluded from the analysis. The longitudinal (E_{axi}) and transverse (E_{trv}) elastic moduli as well as the longitudinal-to-transverse modulus ratio $(E_{\mathrm{axi}}/E_{\mathrm{trv}})$ of the FAY model are calculated for upper and lower bounds of the meaning full range of the individual input parameters, while other parameters are held constant at the operation point. By fitting quadratic functions to the elastic moduli and their ratio with respect to each input parameter, the derivatives of E_{axi}, E_{trv} and $E_{\mathrm{axi}}/E_{\mathrm{trv}}$ are calculated at the operation point. The relative sensitivity is calculated by multiplying the derivatives by the ratio of each input parameter versus the corresponding elastic variable at the operation point. Moreover, the relative change is obtained by dividing the variation of E_{axi}, E_{trv} and $E_{\mathrm{axi}}/E_{\mathrm{trv}}$ over the meaningful range of the input parameters by the corresponding value at the operation point.

2.5 Analytical models

Different analytical models including Voigt and Reuss, Piekarski, shear-lag, Hashin–Shtrikman, and Mori–Tanaka methods are applied to investigate the elastic properties of MCF, EFM and FAY. In the current section, the subscripts m and f, respectively, refer to the matrix and fiber. Similarly,φ, E, G and ν denote volume fraction, elastic modulus, shear modulus and Poisson's ratio, respectively. Mechanical properties of constituents and the composition of each model are selected based on the data presented in Sect. 2.1.

In the analytical model of MCF, HA platelet is assumed as fiber and the collagen as matrix. Besides, the mineral crystals and NCP in EFM, as well as the MCF and EFM in the FAY are considered as fiber and matrix, respectively. It should be emphasized that the results of MCF and EFM models are used as inputs for the FAY in each analytical method. The analytical models that are used in the current study are described below.

The effective longitudinal elastic modulus calculated by the Voigt method (Voigt 1889) in which the composite material is subjected to a uniform strain is given by

$$E_{\mathrm{L}} = \varphi_{\mathrm{f}}E_{\mathrm{f}} + \varphi_{\mathrm{m}}E_{\mathrm{m}}. \tag{6}$$

The Reuss model (Reuss 1929) [Eq. (7)] is used for assessing the effective transverse elastic modulus of composite models considering the material with uniform stress layers of matrix and fiber:

$$\frac{1}{E_{\mathrm{t}}} = \frac{\varphi_{\mathrm{f}}}{E_{\mathrm{f}}} + \frac{\varphi_{\mathrm{m}}}{E_{\mathrm{m}}}. \tag{7}$$

The linear combination of Voigt and Reuss models was employed by Hirsch (1962) which calculated the intermediate properties of composite, being suitable for evaluating the elastic behavior of the bone. In this regard, Piekarski (1973) assumed bone as a two-phase composite and used Hirsch's model (1962) to calculate the longitudinal elastic modulus of bone. In Piekarski's model, the relative proportion of upper and lower bounds of material is defined with x and $(1-x)$ and the value of x is proposed to be 0.925 in bone (Piekarski 1973):

$$\frac{1}{E_{\mathrm{L}}} = x\left(\frac{1}{\varphi_{\mathrm{f}}E_{\mathrm{f}} + \varphi_{\mathrm{m}}E_{\mathrm{m}}}\right) + (1-x)\left(\frac{\varphi_{\mathrm{f}}}{E_{\mathrm{f}}} + \frac{\varphi_{\mathrm{m}}}{E_{\mathrm{m}}}\right). \tag{8}$$

The mechanical model of MCF proposed by Jäger and Fratzl (2000) (shear-lag model) is also considered in the present study, where the staggered mineral bricks are arranged within collagen fibrils. Applying tensile stress in the model indicates that mineral platelets bear the tensile load, while collagen matrix transfers the load between HA crystals in shear. Gao et al. (2003) utilized a one-dimensional serial spring system consisting of mineral and protein elements to estimate the elastic modulus of bone as a composite material. The shear-lag formula in which the aspect ratio of mineral platelets is designated by ρ (Gao et al. 2003) is:

$$\frac{1}{E_{\mathrm{L}}} = \frac{4\left(1-\varphi_{\mathrm{f}}\right)}{G_{\mathrm{m}}\varphi_{\mathrm{f}}^2\rho^2} + \frac{1}{\varphi_{\mathrm{f}}E_{\mathrm{f}}}. \tag{9}$$

In the current study, the axial modulus of both MCF and FAY is obtained and the axial strain ratios s of HA platelets versus MCF and MCF versus FAY are calculated by applying the equation of the shear-lag model twice:

$$s = \frac{1}{1 + \frac{4E_f}{G_m \rho^2} \times \frac{(1-\varphi_f)}{\varphi_f}} \tag{10}$$

In comparison with the Voigt and Reuss models, refined upper and lower bounds of the elastic modulus of a composite can be obtained with the Hashin–Shtrikman theory (1963). The Hashin–Shtrikman (1963) equations are the following:

$$\begin{aligned}
K_{\text{lower}} &= K_m + \frac{\varphi_f}{\frac{1}{K_f - K_m} + \frac{3\varphi_m}{3K_m + 4G_m}} \\
K_{\text{upper}} &= K_f + \frac{\varphi_m}{\frac{1}{K_m - K_f} + \frac{3\varphi_f}{3K_f + 4G_f}} \\
G_{\text{lower}} &= G_m + \frac{\varphi_f}{\frac{1}{G_f - G_m} + \frac{6\varphi_m(K_m + 2G_m)}{5G_m(3K_m + 4G_m)}} \\
G_{\text{upper}} &= G_f + \frac{\varphi_m}{\frac{1}{G_m - G_f} + \frac{6\varphi_f(K_f + 2G_f)}{5G_f(3K_f + 4G_f)}} \\
E_{\text{lower}} &= \frac{9K_{\text{lower}}G_{\text{lower}}}{3K_{\text{lower}} + G_{\text{lower}}} \\
E_{\text{upper}} &= \frac{9K_{\text{upper}}G_{\text{upper}}}{3K_{\text{upper}} + G_{\text{upper}}},
\end{aligned} \tag{11}$$

where K represents the bulk modulus.

The effective stiffness tensors of the three different models are also calculated with the Mori–Tanaka method (Benveniste 1987; Li and Wang 2008; Mortazavi et al. 2013; Tran et al. 2018). In MCF, the collagen is assumed as matrix and hydroxyapatite is considered as inclusion. The flat ellipsoidal inclusions are used for calculating the Eshelby tensor in the MCF model (Eshelby 1957; Withers 1989; Meng et al. 2012; Mura 2013). In the EFM, the NCP is assumed as matrix and mineral platelet is considered as inclusion. Due to the cubic shape of the EFM model, presented in Sect. 2.2.2, spherical inclusions are used for EFM for the analytical estimation (Mura 2013). In the FAY, the EFM and MCF are, respectively, assumed as matrix and inclusion. The circular cylinder inclusions are applied for determining the Eshelby tensors for this model (Mura 2013). The effective stiffness tensor C is calculated with:

$$\begin{aligned}
C =& C_m + \phi_f (C_f - C_m)\left[I + \mathrm{SC}_m^{-1}(C_f - C_m)\right]^{-1} \\
&\left[(1-\phi_f)I + \phi_f\left[I + \mathrm{SC}_m^{-1}(C_f - C_m)\right]^{-1}\right]^{-1},
\end{aligned} \tag{12}$$

where C_m, C_f, S, I and ϕ_f are the stiffness tensor of matrix, stiffness tensor of fiber, Eshelby's tensor, identity tensor and volume fraction of the fibers, respectively.

3 Results

3.1 Calibration with experimental results

The calibrated FEA results for FAY are compared with the experimental results of Casari et al. (2019b) in Table 4. The errors are in the range of 1%.

A mesh convergence study was conducted for the three FE models where the original element size reported above is divided by two. The results indicate that in the MCF model, the axial and transverse elastic moduli decreased by 0.05 and 0.25%, respectively. No changes were noticed in the EFM model and not only the axial and transverse elastic moduli but also the ratio of axial versus transverse moduli changed by less than 0.5% in FAY. The precision of the FE calibration is therefore in the range of the FE precision.

3.2 Mechanical properties of MCF, EFM and FAY with different analytical methods and FEA results

The axial and transverse elastic moduli of MCF, EFM, and FAY computed with analytical approaches and FEA are listed in Table 5. Since the MCF and FAY models are orthotropic, the average of elastic moduli in the two transverse directions is reported as the transverse modulus for both FE and Mori–Tanaka methods. In MCF, the Piekarski model provides a good estimate of axial elastic modulus, while shear-lag delivers a strong underestimation. The elastic properties of EFM are poorly estimated in most analytical calculations. In FAY, the Piekarski model overestimates and the shear lag model underestimates the axial modulus. Upper and lower bounds of the axial or transverse elastic moduli are obtained by the simple Voigt and Reuss models for all unit cells.

The effective orthotropic elastic moduli, shear moduli and Poisson's ratios of MCF, EFM and FAY in FEA and Mori–Tanaka methods along X, Y and Z directions are given in Table 6. In addition, the effective elasticity

Table 4 Comparison between FE (current study) and experimental results (Casari et al. 2019b) of fibril array at the micro scale

Item	Elastic modulus (GPa)		Ratio of elastic modulus $\left(\frac{E_{axi}}{E_{trv}}\right)$
	Axial (E_{axi})	Transverse (E_{trv})	
FEA	29.78	14.86	2.00
Experiment (Casari et al. 2019b)	30.00	15.05	1.99
Error (%)	0.73	1.26	0.50

Table 5. Elastic modulus of MCF, EFM and fibril array calculated with different analytical methods and FEA (GPa)

Model	Item	Axial	Transverse
MCF	Voigt	36.84	–
	Reuss	–	8.33
	Piekarski	29.32	–
	Shear-lag	21.68	–
	Hashin–Shtrikman	24.94	10.39
	Mori–Tanaka	26.39	14.65
	FEA	30.91	12.98
EFM	Voigt	102.55	
	Reuss	8.06	
	Piekarski	54.56	
	Shear-lag	88.50	
	Hashin–Shtrikman	14.62–95.97[a]	
	Mori–Tanaka	14.62	
	FEA	25.34	
FAY	Voigt	49.98	–
	Reuss	–	8.27
	Piekarski	34.20	–
	Shear-lag	17.34	–
	Hashin–Shtrikman	31.60	11.13
	Mori–Tanaka	24.04	14.51
	FEA	29.78	14.86

[a]The lower and upper bounds of Hashin–Shtrikman are presented as transverse and axial elastic modulus, respectively

tensors of MCF, EFM and FAY obtained with the FE and Mori–Tanaka methods are plotted in Fig. 6 to illustrate the differences. The overall stiffness of MCF and FAY are consistent across the two methods, but the axial modulus is underestimated and the shape of the tensors is more anisotropic for the Mori–Tanaka method. Moreover, the Mori–Tanaka method underestimates the elastic modulus and overestimates the shear modulus of EFM.

3.3 Strain ratio

Using FEA, an axial strain ratio of 0.8 is obtained for HA in MCF, and a value of almost 0.99 is found for MCF in FAY. Using the shear lag method, the calculated axial strain ratios are consistently 0.74 and 0.98, respectively.

3.4 Stress distribution

In order to illustrate the load transfer mechanisms between phases, the stress distributions in MCF, EFM, and FAY computed by FEA for 2% apparent tensile strain along the longitudinal direction (Z) are provided in this section. The displayed values of stresses from our linear elastic analyses at this relatively large strain are therefore higher than those expected during an experiment.

3.4.1 Stress distribution in MCF

The stress distribution in Fig. 7 reflects the characteristic of the shear-lag model in which mineral platelets, with higher stiffness compared to the collagen, carry the axial stresses and collagen transfers the load between the HA crystals by shear stresses. Thus, the higher normal stresses appear in hydroxyapatite and the higher shear stresses are sustained by collagen in the MCF model.

3.4.2 Stress distribution in EFM

Normal and shear stresses in the EFM including mineral crystals and NCP are shown in Fig. 8, in which HA crystals sustain higher normal stresses due to their much higher stiffness in comparison with the NCPs.

3.4.3 Stress distribution in FAY

The normal stresses σ_{33} of the FAY cross section at the ends and in the middle region are shown in Fig. 9a, b, respectively. The higher stresses in the MCF compared to the EFM phase confirm that the axial load is mainly sustained by the

Table 6 Elastic and shear moduli and Poisson's ratios of MCF, EFM and FAY obtained with Mori–Tanaka method and FEA (GPa) as well as their differences

Model	Item	E_1	E_2	E_3	G_{23}	G_{13}	G_{12}	ϑ_{23}	ϑ_{31}	ϑ_{12}
MCF	Mori–Tanaka	9.81	19.49	26.39	8.81	3.29	3.30	0.195	0.322	0.179
	FEA	11.66	14.30	30.91	4.67	3.68	3.31	0.126	0.287	0.211
	Δ (%)	15.87	36.29	14.62	88.65	10.60	0.30	54.76	12.19	15.16
EFM	Mori–Tanaka	14.62	14.62	14.62	5.82	5.82	5.82	0.256	0.256	0.256
	FEA	25.34	25.34	25.34	4.44	4.44	4.44	0.079	0.079	0.079
	Δ (%)	42.30	42.30	42.30	31.08	31.08	31.08	224.05	224.05	224.05
FAY	Mori–Tanaka	10.64	18.38	24.04	8.09	3.70	3.68	0.200	0.308	0.193
	FEA	13.68	16.04	29.78	4.62	3.82	3.51	0.123	0.236	0.193
	Δ (%)	22.22	14.59	19.27	75.11	3.14	4.84	62.60	30.51	0

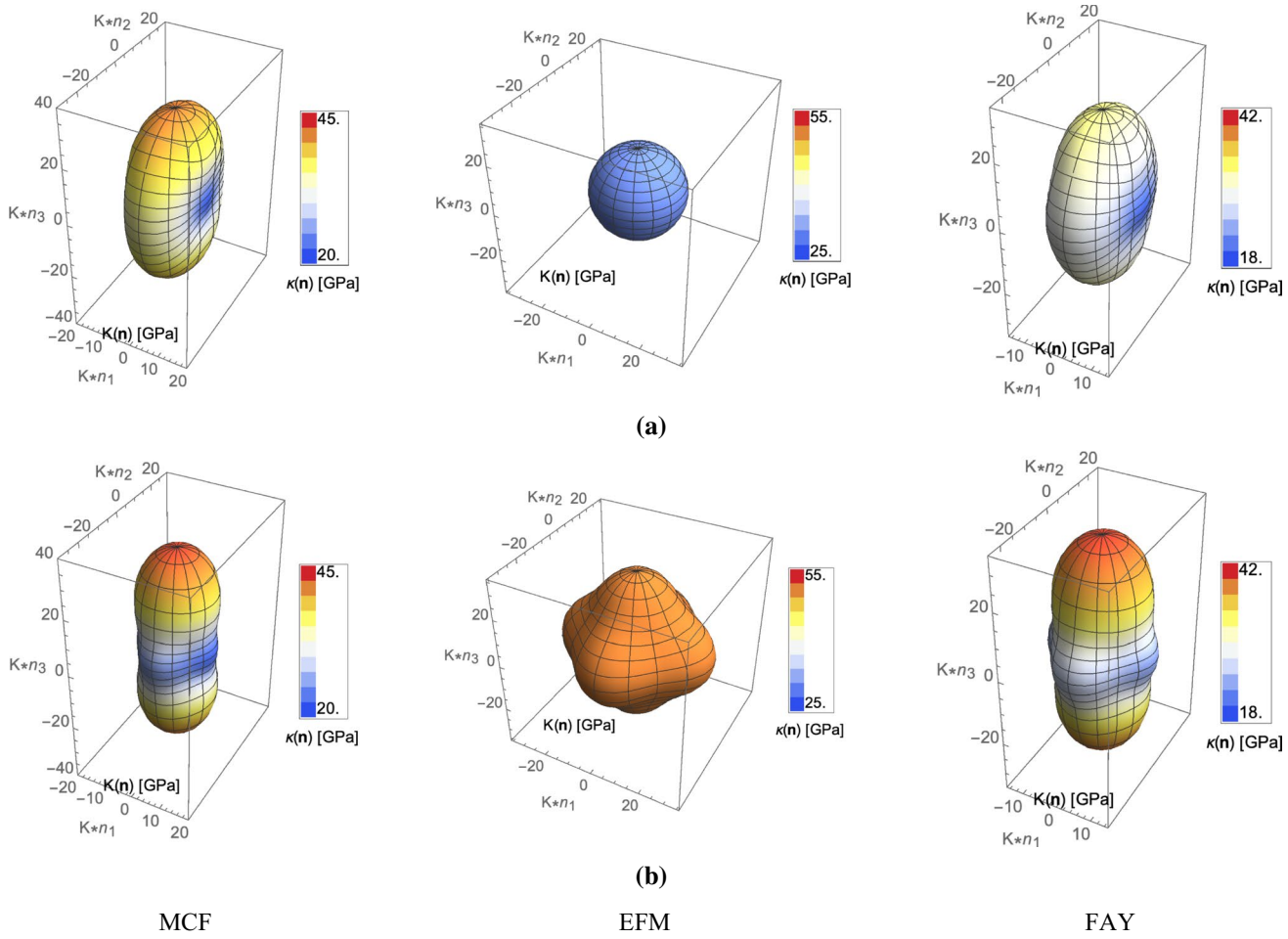

Fig. 6 Plot of the elasticity tensors of MCF, EFM and FAY determined based on **a** Mori–Tanaka method and **b** FEA (Unit: GPa). The location of the surface corresponds to the elongation modulus, and the color designates the bulk modulus for all material directions (He and Curnier 1995)

MCF. As shown in Fig. 9c, the largest normal stresses along the FAY are observed in the middle zone with a stress concentration factor of about 2, which is consistent with the failure mode of the MCF demonstrated in the tensile tests of Casari et al. (2019b).

3.5 Sensitivity analysis

Since the density of hydroxyapatite platelet is assumed approximately 3.1 g/cm^3 (Lees 1987; Hellmich et al. 2004) and the density of collagen and NCP are considered 1.18 g/cm^3 (Piekarski 1973; Cusack and Miller 1979; Deuerling et al. 2009; Gautieri et al. 2011), and thus the meaningful range for mineral volume fraction in FAY is set to 0.4–0.45 in order to maintain tissue density around 2 g/cm^3. Meaningful ranges of variation are also selected for elastic modulus of HA, collagen and also volume fraction of MCF in FAY based on Table 1. On the other hand, the upper bound of NCP elastic modulus (Nikolov and Raabe 2008; Hamed et al. 2012) and aspect ratio of HA (Siegmund et al. 2008; Vercher-Martínez et al. 2015) are selected even higher than the values of Table 1 in order to explore asymptotic trends.

As shown in Table 7, the mineral volume fraction in FAY (φ_{HA}) demonstrates the highest relative sensitivity in both longitudinal and transverse elastic moduli. In turn, the MCF volume fraction in FAY (φ_{MCF}) is the most sensitive parameter for the ratio $(E_{\mathrm{axi}}/E_{\mathrm{trv}})$. Furthermore, the elastic modulus of hydroxyapatite (E_{HA}) and collagen (E_{Collagen}) are the second most sensitive parameters in longitudinal and transverse moduli, respectively.

The relative change of elastic moduli and their ratio shows the relative variation of the input parameters with respect to the selected input parameter range. In fact, NCP elastic modulus delivers the highest relative changes with a range of 0.3–1.8 GPa for the axial and transverse moduli.

Interestingly, the 4 parameters with the highest relative sensitivity of φ_{HA}, φ_{MCF}, E_{HA} and E_{Collagen} exhibited a highly

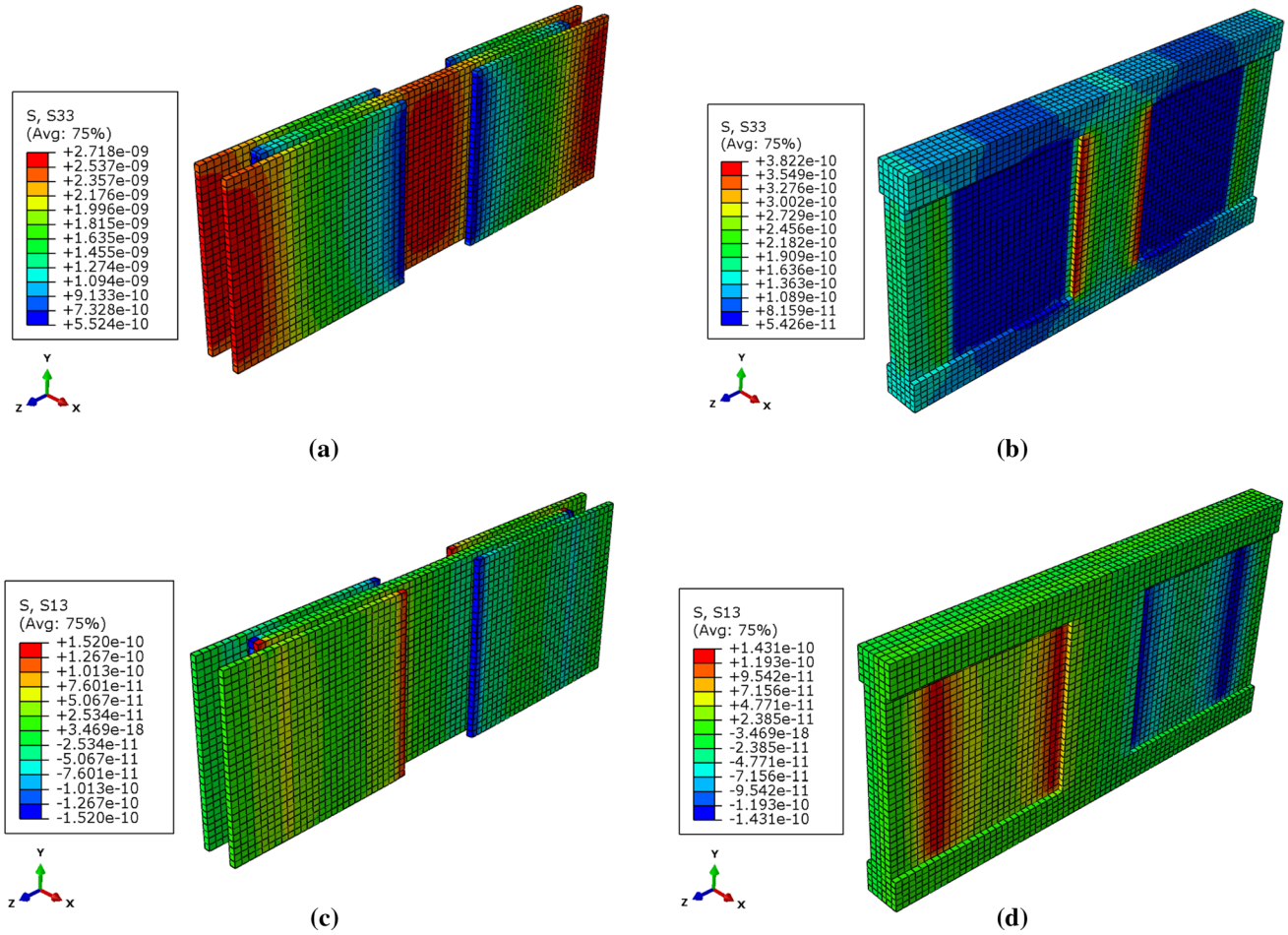

Fig. 7 Stress distribution in the MCF model under 2% tensile loading in the longitudinal direction, **a** normal stress σ_{33} in mineral platelets, **b** normal stress σ_{33} in collagen, **c** shear stress σ_{13} in mineral platelets, **d** shear stress σ_{13} in collagen $\left(\text{Unit:}\frac{\text{N}}{(\text{nm})^2}\right)$

linear behavior, which means that the relative sensitivity did not change significantly in the meaningful range.

The behavior of the 3 least sensitive input parameters is shown in Fig. 10 and suggests that the influence of mineral aspect ratio on the three output variables levels off at the upper bound. The increase in both axial and transverse elastic moduli weakens with increasing NCP elastic modulus, and the increasing NCP volume fraction appears to enhance moderately the ratio of axial versus transverse modulus in the upper range. Furthermore, the bilinear regression models between the four most sensitive parameters reveal that the interactions are either statistically insignificant or quantitatively negligible for E_{axi}, E_{trv} and $E_{\text{axi}}/E_{\text{trv}}$.

4 Discussion and conclusion

The motivation for this research was the development of a computationally efficient FE model of the bone MCF and EFM to investigate the elastic and post-yield properties of the FAY with a maximum of experimental realism and a minimum of assumptions. The present study focused on the design of continuum unit-cell models in which the morphological parameters and material properties are calculated by calibrating the axial and transverse elastic moduli of FAY with state-of-the-art experimental data acquired under dry condition for ovine osteons with approximately parallel mineralized collagen fibrils. Then, a comparison of FEA with previous analytical models was conducted, a sensitivity analysis was undertaken to clarify the role of the various model parameters, and strain ratios between specific phases were calculated.

The proposed FAY model consists of aligned mineralized collagen fibrils (MCF) embedded in an extrafibrillar matrix (EFM). The collagen and hydroxyapatite platelets are the main building blocks of MCF, while additional mineral crystals and NCPs are the constituents of EFM. In these first linear analyses, no delamination between phases or post-yield behavior of the constituents is modeled. Most FE models can be tuned to deliver realistic elastic properties,

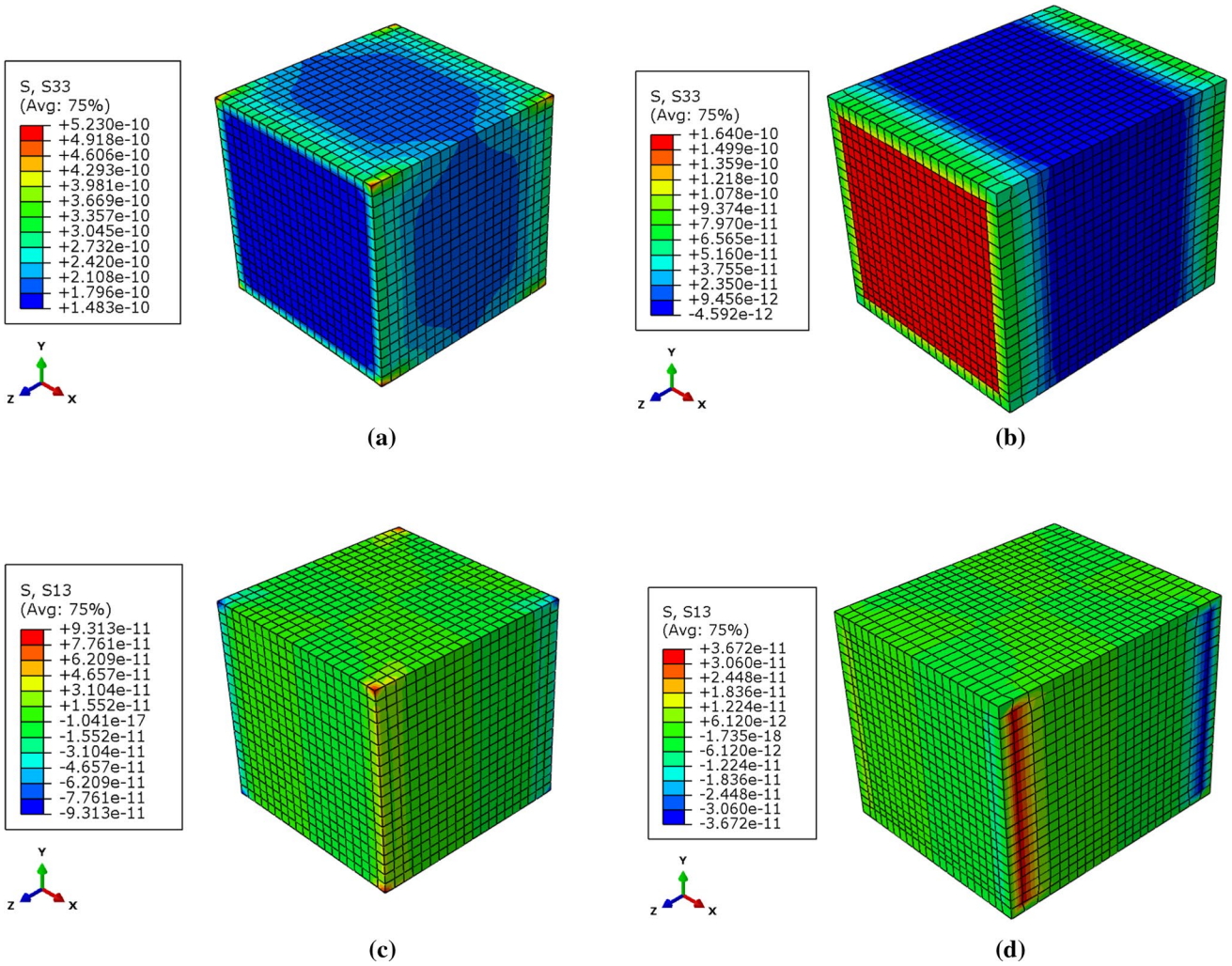

Fig. 8 Stress distribution in the EFM model under 2% tensile loading in the longitudinal direction, **a** normal stress σ_{33} in mineral platelets, **b** normal stress σ_{33} in NCP, **c** shear stress σ_{13} in mineral crystals, **d** shear stress σ_{13} in NCP $\left(\text{Unit:}\frac{\text{N}}{(\text{nm})^2}\right)$

and there is obviously no unique set of material parameters to fit the experiments. Compared to previous FE analyses, the present model represents a true compromise between simplicity and fidelity, is designed to reflect the correct load transfer mechanisms, and delivers accurate elastic properties. The architecture of the unit cells and the composition, dimensions and elastic properties of the constituents are fully compatible with current knowledge of bone ECM. A systematic comparison of two-scale FEA with those of analytical methods is performed from the simplest to the most sophisticated one. The Voigt and Reuss produce the upper and lower bounds for axial versus transverse elastic properties in both MCF and FAY. The shear-lag model involves the correct load transfer but produces lower axial elastic moduli in MCF and FAY, while Hashin and Shtrikman model delivers substantially improved bounds for the FAY. The anisotropic results of the Mori–Tanaka model differ from those of FEA for MCF and FAY and even more so for EFM (Fig. 6), as the architecture of EFM does not fulfill the hypothesis of dilute inclusions underlying the Mori–Tanaka scheme. An alternative homogenization schemes may have to be used for the EFM. The latter geometry was chosen to account for the observed granular morphology of the EFM and to reach the high volume fraction of the mineral phase necessary to achieve the observed elastic properties. The normal and shear stress distributions confirm the shear-lag mechanism proposed by Jäger and Fratzl (2000), which interestingly appears at all MCF, EFM and FAY levels.

In order to get some insight into how different input parameters affect the properties of FAY, a comprehensive sensitivity analysis is conducted on axial and transverse elastic moduli and their ratio with respect to the input parameters. As expected, mineral volume fraction dominates the overall stiffness of the bone FAY. The elastic

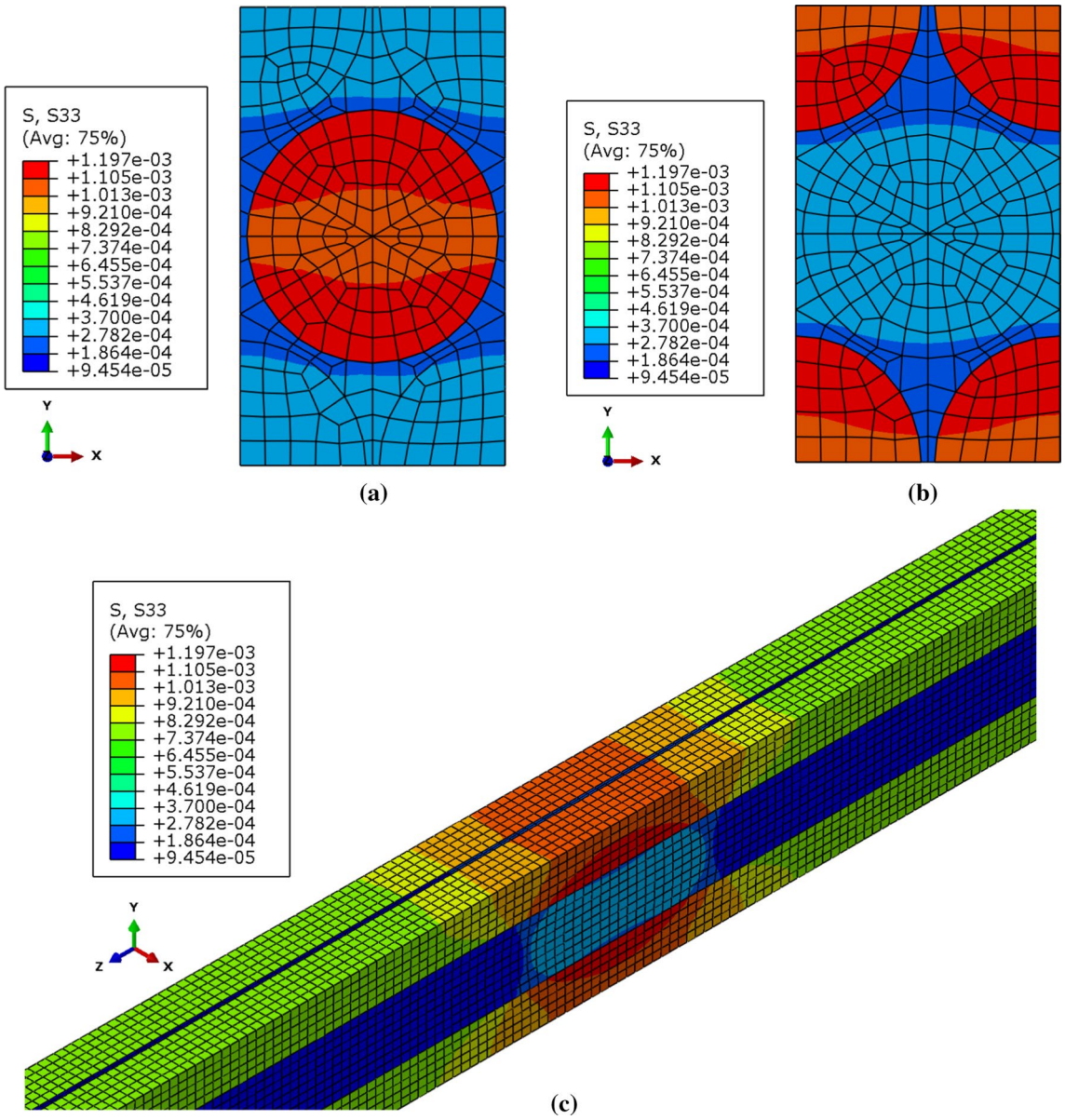

Fig. 9 Normal stress σ_{33} distribution in the FAY under 2% tensile loading in the longitudinal direction, **a** the cross section at the end of fibril array, **b** the cross section in the middle zone of the FAY, **c** the length of the FAY $\left(\text{Unit:}\frac{\text{N}}{(\mu\text{m})^2}\right)$

Table 7 Sensitivity analysis of seven input parameters

Item	Operation point	Meaningful range	Relative sensitivity			Relative change (%)		
			E_{axi}	E_{trv}	E_{axi}/E_{trv}	E_{axi}	E_{trv}	E_{axi}/E_{trv}
E_{HA} (GPa)	110	100–120	**0.672**	0.140	**0.505**	12.206	3.059	9.160
$E_{Collagen}$(GPa)	6	5–7	0.197	**0.686**	−0.500	6.561	22.850	−16.632
E_{NCP}(GPa)	0.6	0.3–1.8	0.135	0.158	−0.025	25.326	26.491	−1.652
φ_{MCF}	0.8	0.7–0.85	0.149	−0.537	**0.658**	2.777	−10.010	12.342
φ_{HA}	0.423	0.4–0.45	**1.190**	**1.146**	0.050	14.070	13.674	0.449
φ_{NCP} /EFM	0.069	0.05–0.3	−0.073	−0.112	0.014	−5.534	−20.185	17.420
a_{HA}	30	14–80	0.099	0.017	0.084	15.161	2.224	13.040

The two highest values for each elastic property are bold

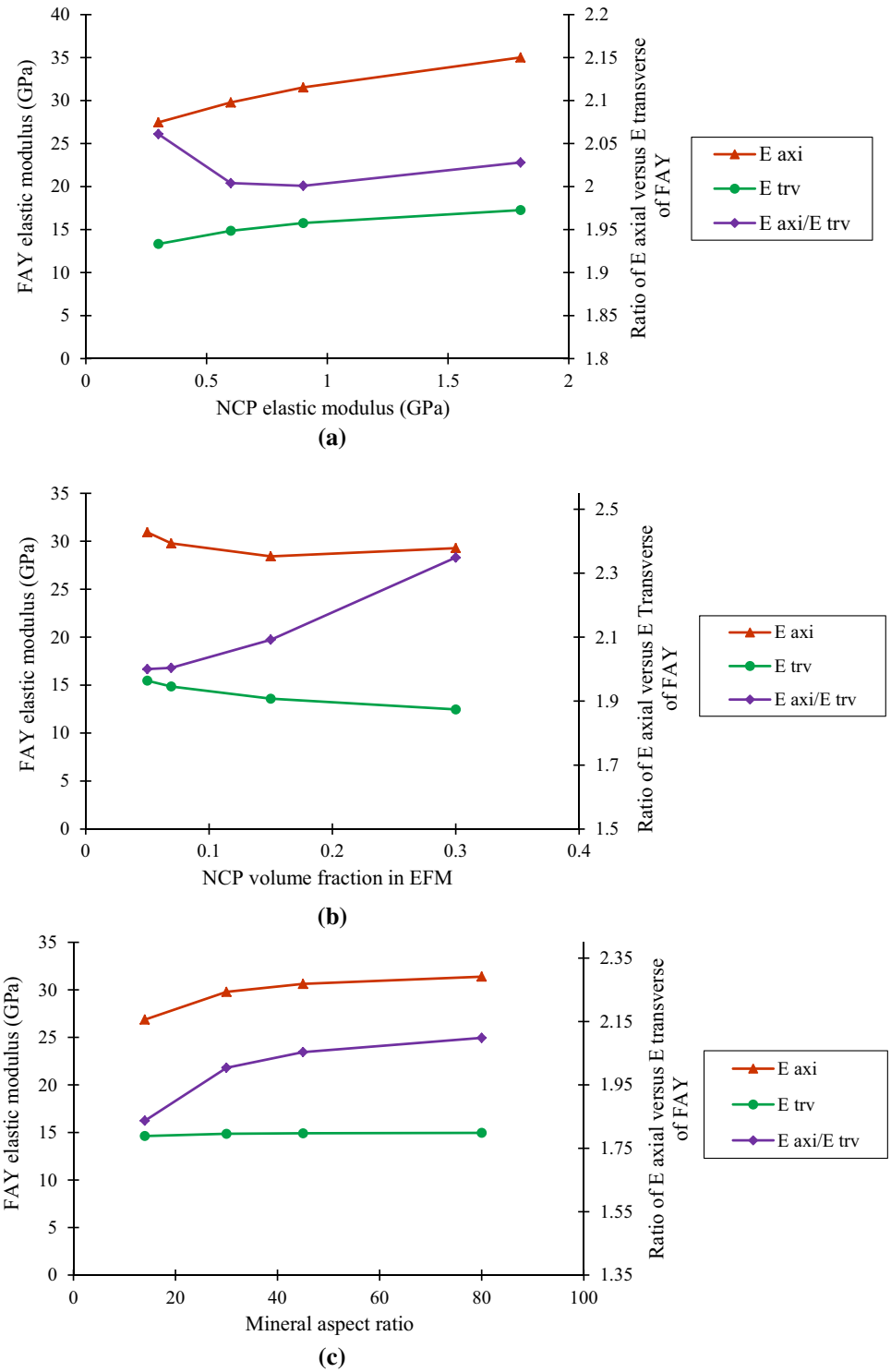

Fig. 10 Axial, transverse and the axial/transverse elastic modulus of FAY versus, **a** NCP elastic modulus, **b** volume fraction of NCP in EFM, **c** aspect ratio of hydroxyapatite

modulus of HA and collagen are also important. In fact, φ_{MCF} could be deduced from the axial versus transverse elastic moduli. The elastic constants E_{axi}, E_{trv} and E_{axi}/E_{trv} were highly linear with respect to the 4 most sensitive parameters φ_{HA}, φ_{MCF}, E_{HA} and $E_{Collagen}$ and minimal if no interaction was found between them. The 3 other parameters have a moderate influence and increasing the mineral aspect ratio has a minimal influence on the elastic properties of the FAY.

Since limited results are available on strain ratios (Reisinger et al. 2010), we calculated the one of HA in MCF and the one of MCF in FAY by both FEA and the shear-lag method. The strain ratios are consistent between the two methods, though much higher than those reported in

experimental studies. A recent analytical study suggests that this discrepancy is mainly associated with the progressive recruitment of MCFs with different pre-strain into a statistical distribution of stretching, sliding and failing MCFs and can therefore not be described by a linear elastic shear-lag or a unit cell model (Groetsch et al. 2019).

Although highly consistent with current knowledge, the proposed FEA approach has some important limitations. First, for the sake of numerical efficiency, all constituents are represented by continua and their molecular nature deliberately ignored. This can be justified by the large size (approximately 100 μm^3) of the tested FAY volumes in micro-sample experiments, by the interest in apparent mechanical properties and the focus on dominant deformation patterns at that particular scale. Clearly, bridges will need to be established between molecular and continuum descriptions, but this endeavor seems still very challenging. Bound water is included in the volume fractions of the organic constituents, and its mechanical role is integrated into the elastic moduli of collagen and NCP. Poroelasticity is not modeled due to the absence of free water within the available validation experiments performed in vacuo. The role of water can be included in the model whenever tensile and compressive results on wet FAYs become available.

Second, the use of a unit cell model misses the role of defects or the statistical distribution of MCFs and material parameters as explored for instance by Wang and Ural (2018). We justify this again by the simplicity of the models, their numerical efficiency and their ability to deliver a 3D deformation pattern for an idealized but representative configuration of an average FAY.

It is noteworthy that the CPU time (4 cores, 18 Gb RAM, 3.06 GHz) for calculating the axial and transverse elastic moduli in FAY using the two-scale FEM is approximately 1 h. This is slower that analytical models, but much faster than statistical FE models of FAYs.

In summary, a computationally efficient two-scale FE model of the bone FAY is proposed that reflects the current knowledge of ECM composition and architecture. Using unit cells with periodic boundary conditions, both axial and transverse elastic moduli of ovine bone are matched accurately to the recent experimental results measured at the FAY scale. The apparent elastic properties of MCF, EFM, and FAY are computed and systematically compared with the predictions of analytical methods. The obtained stress distributions reflect the classical shear-lag model at both MCF and FAY scales. Finally, our extensively validated and efficient FE models will be exploited to investigate the critical damage accumulation mechanisms in tension and compression and to estimate the anisotropic post-yield properties in the bone ECM.

Acknowledgements Philippe Zysset acknowledges grant no 165510 of the Swiss National Science Foundation (SNSF).

References

Abueidda DW, Sabet FA, Jasiuk IM (2017) Modeling of stiffness and strength of bone at nano-scale. J Biomech Eng 139(5):051006

Adams J, Fantner GE, Fisher LW, Hansma PK (2008) Molecular energy dissipation in nano-scale networks of dentin matrix protein 1 is strongly dependent on ion valence. Nanotechnology 19(38):384008

Akiva U, Wagner HD, Weiner S (1998) Modelling the three-dimensional elastic constants of parallel-fibred and lamellar bone. J Mater Sci 33(6):1497–1509

Akkus O (2005) Elastic deformation of mineralized collagen fibrils: an equivalent inclusion based composite model. J Biomech Eng 127(3):383–390

Alexander B, Daulton TL, Genin GM, Lipner J, Pasteris JD, Wopenka B, Thomopoulos S (2012) The nanometre-scale physiology of bone: steric modelling and scanning transmission electron microscopy of collagen–mineral structure. J R Soc Interface 9(73):1774–1786

Al-Qtaitat AI, Aldalaen SM (2014) A review of non-Collagenous proteins; their role in bone. Am J Life Sci 2:351–355

Amaral M, Lopes MA, Silva RF, Santos JD (2002) Densification route and mechanical properties of Si_3N_4–bioglass biocomposites. Biomaterials 23(3):857–862

Aoubiza B, Crolet JM, Meunier A (1996) On the mechanical characterization of compact bone structure using the homogenization theory. J Biomech 29(12):1539–1547

Asgari M, Abi-Rafeh J, Hendy GN, Pasini D (2019) Material anisotropy and elasticity of cortical and trabecular bone in the adult mouse femur via AFM indentation. J Mech Behav Biomed Mater 93:81–92

Barkaoui A, Hambli R (2011) Finite element 3D modeling of mechanical behavior of mineralized collagen microfibrils. J Appl Biomater Biomech 9(3):199–206

Barkaoui A, Hambli R (2014) Nanomechanical properties of mineralised collagen microfibrils based on finite elements method: biomechanical role of cross-links. Comput Methods Biomech Biomed Eng 17(14):1590–1601

Barkaoui A, Chamekh A, Merzouki T, Hambli R, Mkaddem A (2014) Multi-scale approach including microfibril scale to assess elastic constants of cortical bone based on neural network computation and homogenization method. Int J Numer Methods Biomed Eng 30(3):318–338

Barkaoui A, Hambli R, Tavares JMR (2015) Effect of material and structural factors on fracture behaviour of mineralised collagen microfibril using finite element simulation. Comput Methods Biomech Biomed Eng 18(11):1181–1190

Barkaoui A, Tlili B, Vercher-Martínez A, Hambli R (2016) A multiscale modelling of bone ultrastructure elastic proprieties using finite elements simulation and neural network method. Comput Methods Programs Biomed 134:69–78

Benveniste Y (1987) A new approach to the application of Mori–Tanaka's theory in composite materials. Mech Mater 6(2):147–157

Bhowmik R, Katti KS, Katti DR (2007) Mechanics of molecular collagen is influenced by hydroxyapatite in natural bone. J Mater Sci 42(21):8795–8803

Birk DE, Zycband EI, Woodruff S, Winkelmann DA, Trelstad RL (1997) Collagen fibrillogenesis in situ: fibril segments become long fibrils as the developing tendon matures. Dev Dyn Off Publ Am Assoc Anat 208(3):291–298

Bishop N (2016) Bone material properties in osteogenesis imperfecta. J Bone Miner Res 31(4):699–708
Boskey AL (1992) Mineral–-matrix interactions in bone and cartilage. Clin Orthop Relat Res 281:244–274
Budiansky B (1965) On the elastic moduli of some heterogeneous materials. J Mech Phys Solids 13(4):223–227
Buehler MJ (2006) Atomistic and continuum modeling of mechanical properties of collagen: elasticity, fracture, and self-assembly. J Mater Res 21(8):1947–1961
Buehler MJ (2007) Molecular nanomechanics of nascent bone: fibrillar toughening by mineralization. Nanotechnology 18(29):295102
Buehler MJ (2008) Nanomechanics of collagen fibrils under varying cross-link densities: atomistic and continuum studies. J Mech Behav Biomed Mater 1(1):59–67
Buehler MJ, Keten S, Ackbarow T (2008) Theoretical and computational hierarchical nanomechanics of protein materials: deformation and fracture. Prog Mater Sci 53(8):1101–1241
Casari D, Pethö L, Schürch P, Maeder X, Philippe L, Michler J, Zysset P, Schwiedrzik J (2019a) A self-aligning microtensile setup: Application to single-crystal GaAs microscale tension–compression asymmetry. J Mater Res 34(14):2517–2534
Casari D, Michler J, Zysset P, Schwiedrzik J (2019b) A study of anisotropic strength tension–compression asymmetry in bone extracellular matrix. In: 25th congress of European society of biomechanics, July, 7–10, Vienna, Austria
Cassella JP, Stamp TCB, Ali SY (1996) A morphological and ultrastructural study of bone in osteogenesis imperfecta. Calcif Tissue Int 58(3):155–165
Cowin SC (2001) Bone mechanics handbook. CRC Press, Boca Raton
Cox HL (1952) The elasticity and strength of paper and other fibrous materials. Br J Appl Phys 3(3):72
Cribb AM, Scott JE (1995) Tendon response to tensile stress: an ultrastructural investigation of collagen: proteoglycan interactions in stressed tendon. J Anat 187(Pt 2):423
Currey JD (1969) The relationship between the stiffness and the mineral content of bone. J Biomech 2(4):477–480
Currey JD (2013) Bones: structure and mechanics. Princeton University Press, Princeton
Cusack S, Miller A (1979) Determination of the elastic constants of collagen by Brillouin light scattering. J Mol Biol 135(1):39–51
Deuerling JM, Yue W, Orías AAE, Roeder RK (2009) Specimen-specific multi-scale model for the anisotropic elastic constants of human cortical bone. J Biomech 42(13):2061–2067
Dong XN, Guo XE (2006) Prediction of cortical bone elastic constants by a two-level micromechanical model using a generalized self-consistent method. J Biomech Eng 128(3):309–316
Dubey DK, Tomar V (2008) Microstructure dependent dynamic fracture analyses of trabecular bone based on nascent bone atomistic simulations. Mech Res Commun 35(1–2):24–31
Eppell SJ, Tong W, Katz JL, Kuhn L, Glimcher MJ (2001) Shape and size of isolated bone mineralites measured using atomic force microscopy. J Orthop Res 19(6):1027–1034
Eppell SJ, Smith BN, Kahn H, Ballarini R (2005) Nano measurements with micro-devices: mechanical properties of hydrated collagen fibrils. J R Soc Interface 3(6):117–121
Eshelby JD (1957) The determination of the elastic field of an ellipsoidal inclusion, and related problems. Proc R Soc Lond Ser A Math Phys Sci 241(1226):376–396
Fantner GE, Hassenkam T, Kindt JH, Weaver JC, Birkedal H, Pechenik L, Cutroni JA, Cidade GA, Stucky GD, Morse DE, Hansma PK (2005) Sacrificial bonds and hidden length dissipate energy as mineralized fibrils separate during bone fracture. Nat Mater 4(8):612
Fantner GE, Adams J, Turner P, Thurner PJ, Fisher LW, Hansma PK (2007) Nano-scale ion mediated networks in bone: osteopontin can repeatedly dissipate large amounts of energy. Nano Lett 7(8):2491–2498
Franzoso G, Zysset PK (2009) Elastic anisotropy of human cortical bone secondary osteons measured by nanoindentation. J Biomech Eng 131(2):021001
Fratzl P (2003) Small-angle scattering in materials science-a short review of applications in alloys, ceramics and composite materials. J Appl Crystallogr 36(3):397–404
Fratzl P, Weinkamer R (2007) Nature's hierarchical materials. Prog Mater Sci 52(8):1263–1334
Fratzl P, Groschner M, Vogl G, Plenk H Jr, Eschberger J, Fratzl-Zelman N, Koller K, Klaushofer K (1992) Mineral crystals in calcified tissues: a comparative study by SAXS. J Bone Miner Res 7(3):329–334
Fratzl P, Schreiber S, Boyde A (1996) Characterization of bone mineral crystals in horse radius by small-angle X-ray scattering. Calcif Tissue Int 58(5):341–346
Fratzl P, Gupta HS, Paschalis EP, Roschger P (2004) Structure and mechanical quality of the collagen–mineral nano-composite in bone. J Mater Chem 14(14):2115–2123
Fratzl-Zelman N, Schmidt I, Roschger P, Glorieux FH, Klaushofer K, Fratzl P, Rauch F, Wagermaier W (2014) Mineral particle size in children with osteogenesis imperfecta type I is not increased independently of specific collagen mutations. Bone 60:122–128
Fritsch A, Hellmich C (2007) Universal microstructural patterns in cortical and trabecular, extracellular and extravascular bone materials: micromechanics-based prediction of anisotropic elasticity. J Theor Biol 244(4):597–620
Gao H, Ji B, Jäger IL, Arzt E, Fratzl P (2003) Materials become insensitive to flaws at nano-scale: lessons from nature. Proc Natl Acad Sci 100(10):5597–5600
Gautieri A, Vesentini S, Redaelli A, Buehler MJ (2011) Hierarchical structure and nanomechanics of collagen microfibrils from the atomistic scale up. Nano Lett 11(2):757–766
Giraud-Guille MM (1988) Twisted plywood architecture of collagen fibrils in human compact bone osteons. Calcif Tissue Int 42(3):167–180
Grant CA, Brockwell DJ, Radford SE, Thomson NH (2008) Effects of hydration on the mechanical response of individual collagen fibrils. Appl Phys Lett 92(23):233902
Groetsch A, Zysset PK, Pacareanu A, Peyrin F, Wolfram U (2019) An experimentally informed statistical model for the mechanical behaviour of mineralised collagen fibres. In: 25th congress of European society of biomechanics, July, 7–10, Vienna, Austria
Gupta HS, Seto J, Wagermaier W, Zaslansky P, Boesecke P, Fratzl P (2006) Cooperative deformation of mineral and collagen in bone at the nano-scale. Proc Natl Acad Sci 103(47):17741–17746
Halpin JC, Kardos JL (1976) The Halpin-Tsai equations: a review. Polym Eng Sci 16(5):344–352
Hamed E, Lee Y, Jasiuk I (2010) Multi-scale modeling of elastic properties of cortical bone. Acta Mech 213(1–2):131–154
Hamed E, Novitskaya E, Li J, Chen PY, Jasiuk I, McKittrick J (2012) Elastic moduli of untreated, demineralized and deproteinized cortical bone: validation of a theoretical model of bone as an interpenetrating composite material. Acta Biomater 8(3):1080–1092
Hang F, Barber AH (2010) Nano-mechanical properties of individual mineralized collagen fibrils from bone tissue. J R Soc Interface 8(57):500–505
Hang F, Gupta HS, Barber AH (2014) Nanointerfacial strength between non-collagenous protein and collagen fibrils in antler bone. J R Soc Interface 11(92):20130993
Hansma PK, Fantner GE, Kindt JH, Thurner PJ, Schitter G, Turner PJ, Udwin SF, Finch MM (2005) Sacrificial bonds in the interfibrillar matrix of bone. J Musculoskelet Neuronal Interact 5(4):313

Harley R, James D, Miller A, White JW (1977) Phonons and the elastic moduli of collagen and muscle. Nature 267(5608):285
Hashin Z, Shtrikman S (1963) A variational approach to the theory of the elastic behaviour of multiphase materials. J Mech Phys Solids 11(2):127–140
Hassenkam T, Fantner GE, Cutroni JA, Weaver JC, Morse DE, Hansma PK (2004) High-resolution AFM imaging of intact and fractured trabecular bone. Bone 35(1):4–10
He QC, Curnier A (1995) A more fundamental approach to damaged elastic stress-strain relations. Int J Solids Struct 32(10):1433–1457
Heim AJ, Matthews WG, Koob TJ (2006) Determination of the elastic modulus of native collagen fibrils via radial indentation. Appl Phys Lett 89(18):181902
Hellmich C, Barthélémy JF, Dormieux L (2004) Mineral–collagen interactions in elasticity of bone ultrastructure–a continuum micromechanics approach. Eur J Mech A/Solids 23(5):783–810
Hershey AV (1954) The elasticity of an isotropic aggregate of anisotropic cubic crystals. J Appl Mech Trans ASME 21(3):236–240
Hibbitt K (2013) ABAQUS: user's manual: version 6.13
Hill R (1963) Elastic properties of reinforced solids: some theoretical principles. J Mech Phys Solids 11(5):357–372
Hirsch TJ (1962) Modulus of elasticity of concrete affected by elastic moduli of cement paste matrix and aggregate. In: Journal proceedings, vol 59, no 3, pp 427–452
Hofmann H, Voss T, Kühn K, Engel J (1984) Localization of flexible sites in thread-like molecules from electron micrographs: comparison of interstitial, basement membrane and intima collagens. J Mol Biol 172(3):325–343
Huang J, Wang X, Zhang TL, Wang K (2009) Alterations of ovariectomized rat bone and impact of non-collagenous proteins on mineralization. Joint Bone Spine 76(2):176–183
Ingram RT, Clarke BL, Fisher LW, Fitzpatrick LA (1993) Distribution of noncollagenous proteins in the matrix of adult human bone: evidence of anatomic and functional heterogeneity. J Bone Miner Res 8(9):1019–1029
Jackson SA, Cartwright AG, Lewis D (1978) The morphology of bone mineral crystals. Calcif Tissue Res 25(1):217–222
Jäger I, Fratzl P (2000) Mineralized collagen fibrils: a mechanical model with a staggered arrangement of mineral particles. Biophys J 79(4):1737–1746
Jasiuk I, Ostoja-Starzewski M (2004) Modeling of bone at a single lamella level. Biomech Model Mechanobiol 3(2):67–74
Ji B, Gao H (2004) Mechanical properties of nanostructure of biological materials. J Mech Phys Solids 52(9):1963–1990
Kadler KE, Holmes DF, Trotter JA, Chapman JA (1996) Collagen fibril formation. Biochem J 316(1):1–11
Kasugai S, Todescan R Jr, Nagata T, Yao KL, Butler WT, Sodek J (1991) Expression of bone matrix proteins associated with mineralized tissue formation by adult rat bone marrow cells in vitro: inductive effects of dexamethasone on the osteoblastic phenotype. J Cell Physiol 147(1):111–120
Katz JL (1971) Hard tissue as a composite material—I. Bounds on the elastic behavior. J Biomech 4(5):455–473
Katz EP, Li ST (1973a) The intermolecular space of reconstituted collagen fibrils. J Mol Biol 73(3):351–369
Katz EP, Li ST (1973b) Structure and function of bone collagen fibrils. J Mol Biol 80(1):1–15
Katz JL, Ukraincik K (1971) On the anisotropic elastic properties of hydroxyapatite. J Biomech 4(3):221–227
Kröner E (1958) Berechnung der elastischen Konstanten des Vielkristalls aus den Konstanten des Einkristalls. Z Phys 151(4):504–518
Landis WJ (1996) Mineral characterization in calcifying tissues: atomic, molecular and macromolecular perspectives. Connect Tissue Res 34(4):239–246
Landis S, Price PA (1986) Disaggregation of bone into crystals. Calcif Tissue Int 39(6):365–375
Landis WJ, Silver FH (2002) The structure and function of normally mineralizing avian tendons. Comp Biochem Physiol A Mol Integr Physiol 133(4):1135–1157
Landis WJ, Song MJ, Leith A, McEwen L, McEwen BF (1993) Mineral and organic matrix interaction in normally calcifying tendon visualized in three dimensions by high-voltage electron microscopic tomography and graphic image reconstruction. J Struct Biol 110(1):39–54
Landis WJ, Hodgens KJ, Arena J, Song MJ, McEwen BF (1996) Structural relations between collagen and mineral in bone as determined by high voltage electron microscopic tomography. Microsc Res Tech 33(2):192–202
Lees S (1987) Considerations regarding the structure of the mammalian mineralized osteoid from viewpoint of the generalized packing model. Connect Tissue Res 16(4):281–303
Lees S, Prostak KS, Ingle VK, Kjoller K (1994) The loci of mineral in turkey leg tendon as seen by atomic force microscope and electron microscopy. Calcif Tissue Int 55(3):180–189
Li S, Wang G (2008) Introduction to micromechanics and nanomechanics. World Scientific Publishing Company, Singapore
Lorenzo AC, Caffarena ER (2005) Elastic properties, Young's modulus determination and structural stability of the tropocollagen molecule: a computational study by steered molecular dynamics. J Biomech 38(7):1527–1533
Lusis J, Woodhams RT, Xanthos M (1973) The effect of flake aspect ratio on the flexural properties of mica reinforced plastics. Polym Eng Sci 13(2):139–145
Maghsoudi-Ganjeh M, Lin L, Wang X, Zeng X (2019) Computational investigation of ultrastructural behavior of bone using a cohesive finite element approach. Biomech Model Mechanobiol 18(2):463–478
Mann S, Webb JM, Williams RJP (eds) (1989) Biomineralization: chemical and biochemical perspectives. Wiley, Hoboken
Mbuyi-Muamba JM, Dequeker J, Gevers G (1989) Collagen and non-collagenous proteins in different mineralization stages of human femur. Cells Tissues Organs 134(4):265–268
McNally EA, Schwarcz HP, Botton GA, Arsenault AL (2012) A model for the ultrastructure of bone based on electron microscopy of ion-milled sections. PLoS ONE 7(1):e29258
McNally E, Nan F, Botton GA, Schwarcz HP (2013) Scanning transmission electron microscopic tomography of cortical bone using Z-contrast imaging. Micron 49:46–53
Meng C, Heltsley W, Pollard DD (2012) Evaluation of the Eshelby solution for the ellipsoidal inclusion and heterogeneity. Comput Geosci 40:40–48
Miller A (1984) Collagen: the organic matrix of bone. Philos Trans R Soc Lond B Biol Sci 304(1121):455–477
Minary-Jolandan M, Yu MF (2009a) Nano-scale characterization of isolated individual type I collagen fibrils: polarization and piezoelectricity. Nanotechnology 20(8):085706
Minary-Jolandan M, Yu MF (2009b) Nanomechanical heterogeneity in the gap and overlap regions of type I collagen fibrils with implications for bone heterogeneity. Biomacromol 10(9):2565–2570
MJ S, BF M (1993) Mineral and organic matrix interaction in normally calcifying tendon visualized in 3 dimensions by high-voltage electron-microscopic tomography and graphic image-reconstruction. J Struct Biol 110(1):39–54
Morgan S, Poundarik AA, Vashishth D (2015) Do non-collagenous proteins affect skeletal mechanical properties? Calcif Tissue Int 97(3):281–291
Mori T, Tanaka K (1973) Average stress in matrix and average elastic energy of materials with misfitting inclusions. Acta Metall 21(5):571–574

Mortazavi B, Baniassadi M, Bardon J, Ahzi S (2013) Modeling of two-phase random composite materials by finite element, Mori-Tanaka and strong contrast methods. Compos B Eng 45(1):1117–1125

Mura T (2013) Micromechanics of defects in solids. Springer, Berlin

Nair AK, Gautieri A, Chang SW, Buehler MJ (2013) Molecular mechanics of mineralized collagen fibrils in bone. Nat Commun 4:1724

Nanci A (1999) Content and distribution of noncollagenous matrix proteins in bone and cementum: relationship to speed of formation and collagen packing density. J Struct Biol 126(3):256–269

Nikel O, Laurencin D, McCallum SA, Gundberg CM, Vashishth D (2013) NMR investigation of the role of osteocalcin and osteopontin at the organic–inorganic interface in bone. Langmuir 29(45):13873–13882

Nikel O, Poundarik AA, Bailey S, Vashishth D (2018) Structural role of osteocalcin and osteopontin in energy dissipation in bone. J Biomech 80:45–52

Nikolov S, Raabe D (2008) Hierarchical modeling of the elastic properties of bone at submicron scales: the role of extrafibrillar mineralization. Biophys J 94(11):4220–4232

Olszta MJ, Cheng X, Jee SS, Kumar R, Kim YY, Kaufman MJ, Douglas EP, Gower LB (2007) Bone structure and formation: a new perspective. Mater Sci Eng R Rep 58(3–5):77–116

Orgel JP, Miller A, Irving TC, Fischetti RF, Hammersley AP, Wess TJ (2001) The in situ supermolecular structure of type I collagen. Structure 9(11):1061–1069

Padawer GE, Beecher N (1970) On the strength and stiffness of planar reinforced plastic resins. Polym Eng Sci 10(3):185–192

Paris O, Zizak I, Lichtenegger H, Roschger P, Klaushofer K, Fratzl P (2000) Analysis of the hierarchical structure of biological tissues by scanning X-ray scattering using a micro-beam. Cell Mol Biol (Noisy-le-Grand, France) 46(5):993–1004

Parnell WJ, Grimal Q (2008) The influence of mesoscale porosity on cortical bone anisotropy. Investigations via asymptotic homogenization. J R Soc Interface 6(30):97–109

Parry DA (1988) The molecular fibrillar structure of collagen and its relationship to the mechanical properties of connective tissue. Biophys Chem 29(1–2):195–209

Paschalis EP, Gamsjaeger S, Fratzl-Zelman N, Roschger P, Masic A, Brozek W, Hassler N, Glorieux FH, Rauch F, Klaushofer K, Fratzl P (2016) Evidence for a role for nanoporosity and pyridinoline content in human mild osteogenesis imperfecta. J Bone Miner Res 31(5):1050–1059

Piekarski K (1973) Analysis of bone as a composite material. Int J Eng Sci 11(6):557–565

Poundarik A, Karim L, Gundberg C, Vashishth D (2009) The role of osteocalcin in bone fracture. In: Proceedings of the 55th meeting of the orthopaedic research society, pp 22–25

Poundarik AA, Diab T, Sroga GE, Ural A, Boskey AL, Gundberg CM, Vashishth D (2012) Dilatational band formation in bone. Proc Natl Acad Sci 109(47):19178–19183

Prostak KS, Lees S (1996) Visualization of crystal-matrix structure. In situ demineralization of mineralized turkey leg tendon and bone. Calcif Tissue Int 59(6):474–479

Qiu SR, Wierzbicki A, Orme CA, Cody AM, Hoyer JR, Nancollas GH, Zepeda S, De Yoreo JJ (2004) Molecular modulation of calcium oxalate crystallization by osteopontin and citrate. Proc Natl Acad Sci 101(7):1811–1815

Raspanti M, Congiu T, Guizzardi S (2002) Structural aspects of the extracellular matrix of the tendon: an atomic force and scanning electron microscopy study. Arch Histol Cytol 65(1):37–43

Ravaglioli A, Krajewski A (1991) Bioceramics: materials·properties applications. Springer, Berlin

Reisinger AG, Pahr DH, Zysset PK (2010) Sensitivity analysis and parametric study of elastic properties of a unidirectional mineralized bone fibril-array using mean field methods. Biomech Model Mechanobiol 9(5):499–510

Reisinger AG, Pahr DH, Zysset PK (2011a) Principal stiffness orientation and degree of anisotropy of human osteons based on nanoindentation in three distinct planes. J Mech Behav Biomed Mater 4(8):2113–2127

Reisinger AG, Pahr DH, Zysset PK (2011b) Elastic anisotropy of bone lamellae as a function of fibril orientation pattern. Biomech Model Mechanobiol 10(1):67–77

Reuss A (1929) Berechnung der fließgrenze von mischkristallen auf grund der plastizitätsbedingung für einkristalle. ZAMM J Appl Math Mech/Z Angew Math Mech 9(1):49–58

Reznikov N, Shahar R, Weiner S (2014) Bone hierarchical structure in three dimensions. Acta Biomater 10(9):3815–3826

Reznikov N, Bilton M, Lari L, Stevens MM, Kröger R (2018) Fractal-like hierarchical organization of bone begins at the nanoscale. Science 360(6388):eaao2189

Rho JY, Kuhn-Spearing L, Zioupos P (1998) Mechanical properties and the hierarchical structure of bone. Med Eng Phys 20(2):92–102

Rice RV, Casassa EF, Kerwin RE, Maser MD (1964) On the length and molecular weight of tropocollagen from calf skin. Arch Biochem Biophys 105(2):409–423

Ritchie RO, Buehler MJ, Hansma P (2009) Plasticity and toughness in bone. Phys Today 62(6):41–47

Roach HI (1994) Why does bone matrix contain non-collagenous proteins? The possible roles of osteocalcin, osteonectin, osteopontin and bone sialoprotein in bone mineralisation and resorption. Cell Biol Int 18(6):617–628

Robinson RA (1952) An electron-microscopic study of the crystalline inorganic component of bone and its relationship to the organic matrix. JBJS 34(2):389–476

Rubin MA, Jasiuk I, Taylor J, Rubin J, Ganey T, Apkarian RP (2003) TEM analysis of the nanostructure of normal and osteoporotic human trabecular bone. Bone 33(3):270–282

Sasaki N, Odajima S (1996) Stress–strain curve and Young's modulus of a collagen molecule as determined by the X-ray diffraction technique. J Biomech 29(5):655–658

Sasaki N, Sudoh Y (1997) X-ray pole figure analysis of apatite crystals and collagen molecules in bone. Calcif Tissue Int 60(4):361–367

Schwarcz HP, McNally EA, Botton GA (2014) Dark-field transmission electron microscopy of cortical bone reveals details of extrafibrillar crystals. J Struct Biol 188(3):240–248

Schwarcz HP, Abueidda D, Jasiuk I (2017) The ultrastructure of bone and its relevance to mechanical properties. Front Phys 5:39

Schwiedrzik J, Raghavan R, Bürki A, LeNader V, Wolfram U, Michler J, Zysset P (2014) In situ micropillar compression reveals superior strength and ductility but an absence of damage in lamellar bone. Nat Mater 13(7):740

Shen ZL, Dodge MR, Kahn H, Ballarini R, Eppell SJ (2010) In vitro fracture testing of submicron diameter collagen fibril specimens. Biophys J 99(6):1986–1995

Siegmund T, Allen MR, Burr DB (2008) Failure of mineralized collagen fibrils: modeling the role of collagen cross-linking. J Biomech 41(7):1427–1435

Silver FH, Freeman JW, Seehra GP (2003) Collagen self-assembly and the development of tendon mechanical properties. J Biomech 36(10):1529–1553

Spiesz EM, Zysset PK (2015) Structure–mechanics relationships in mineralized tendons. J Mech Behav Biomed Mater 1(52):72–84

Sroga GE, Vashishth D (2012) Effects of bone matrix proteins on fracture and fragility in osteoporosis. Curr Osteoporos Rep 10(2):141–150

Stevens MJ (2008) Simulation of the mechanical strength of a single collagen molecule. Biophys J 95(1):33–39

Tang Y, Ballarini R, Buehler MJ, Eppell SJ (2009) Deformation micromechanisms of collagen fibrils under uniaxial tension. J R Soc Interface 7(46):839–850

Tertuliano OA, Greer JR (2016) The nanocomposite nature of bone drives its strength and damage resistance. Nat Mater 15(11):1195

Thurner PJ (2009) Atomic force microscopy and indentation force measurement of bone. Wiley Interdiscip Rev Nanomed Nanobiotechnol 1(6):624–649

Thurner PJ, Chen CG, Ionova-Martin S, Sun L, Harman A, Porter A, Ager JW III, Ritchie RO, Alliston T (2010) Osteopontin deficiency increases bone fragility but preserves bone mass. Bone 46(6):1564–1573

Tran VP, Brisard S, Guilleminot J, Sab K (2018) Mori-Tanaka estimates of the effective elastic properties of stress-gradient composites. Int J Solids Struct 146:55–68

Traub W, Arad T, Weiner S (1989) Three-dimensional ordered distribution of crystals in turkey tendon collagen fibers. Proc Natl Acad Sci 86(24):9822–9826

Urist MR, Strates BS (2009) The classic: bone morphogenetic protein. Clin Orthop Relat Res® 467(12):3051

Van Der Rijt JA, Van Der Werf KO, Bennink ML, Dijkstra PJ, Feijen J (2006) Micromechanical testing of individual collagen fibrils. Macromol Biosci 6(9):697–702

Vercher A, Giner E, Arango C, Tarancón JE, Fuenmayor FJ (2014) Homogenized stiffness matrices for mineralized collagen fibrils and lamellar bone using unit cell finite element models. Biomech Model Mechanobiol 13(2):437–449

Vercher-Martínez A, Giner E, Arango C, Fuenmayor FJ (2015) Influence of the mineral staggering on the elastic properties of the mineralized collagen fibril in lamellar bone. J Mech Behav Biomed Mater 42:243–256

Vesentini S, Fitié CF, Montevecchi FM, Redaelli A (2005) Molecular assessment of the elastic properties of collagen-like homotrimer sequences. Biomech Model Mechanobiol 3(4):224–234

Voigt W (1889) Ueber die Beziehung zwischen den beiden Elasticitätsconstanten isotroper Körper. Ann Phys 274(12):573–587

Wagner HD, Weiner S (1992) On the relationship between the microstructure of bone and its mechanical stiffness. J Biomech 25(11):1311–1320

Wall P (1997) A comparison of homogenization, Hashin-Shtrikman bounds and the Halpin-Tsai equations. Appl Math 42(4):245–257

Wallace JM (2012) Applications of atomic force microscopy for the assessment of nano-scale morphological and mechanical properties of bone. Bone 50(1):420–427

Wang Y, Ural A (2018) Mineralized collagen fibril network spatial arrangement influences cortical bone fracture behavior. J Biomech 66:70–77

Weiner S, Traub W (1986) Organization of hydroxyapatite crystals within collagen fibrils. FEBS Lett 206(2):262–266

Weiner S, Traub W (1992) Bone structure: from angstroms to microns. FASEB J 6(3):879–885

Weiner S, Traub W, Wagner HD (1999) Lamellar bone: structure–function relations. J Struct Biol 126(3):241–255

Wenger MP, Bozec L, Horton MA, Mesquida P (2007) Mechanical properties of collagen fibrils. Biophys J 93(4):1255–1263

Wise ER, Maltsev S, Davies ME, Duer MJ, Jaeger C, Loveridge N, Murray RC, Reid DG (2007) The organic–mineral interface in bone is predominantly polysaccharide. Chem Mater 19(21):5055–5057

Withers PJ (1989) The determination of the elastic field of an ellipsoidal inclusion in a transversely isotropic medium, and its relevance to composite materials. Philos Mag A 59(4):759–781

Wu W, Owino J, Al-Ostaz A, Cai L (2014) Applying periodic boundary conditions in finite element analysis. In: SIMULIA community conference, Providence, pp 707–719

Yang L, van der Werf KO, Koopman BF, Subramaniam V, Bennink ML, Dijkstra PJ, Feijen J (2007) Micromechanical bending of single collagen fibrils using atomic force microscopy. J Biomed Mater Res Part A 82(1):160–168

Yang L, Van der Werf KO, Fitié CF, Bennink ML, Dijkstra PJ, Feijen J (2008) Mechanical properties of native and cross-linked type I collagen fibrils. Biophys J 94(6):2204–2211

Yao H, Ouyang L, Ching WY (2007) Ab initio calculation of elastic constants of ceramic crystals. J Am Ceram Soc 90(10):3194–3204

Yuan F, Stock SR, Haeffner DR, Almer JD, Dunand DC, Brinson LC (2011) A new model to simulate the elastic properties of mineralized collagen fibril. Biomech Model Mechanobiol 10(2):147–160

Zappone B, Thurner PJ, Adams J, Fantner GE, Hansma PK (2008) Effect of Ca^{2+} ions on the adhesion and mechanical properties of adsorbed layers of human osteopontin. Biophys J 95(6):2939–2950